D5.4   THE PASSION METRO RECONFIGURABLE OPTICAL NETWORK

Project title	**Photonics technologies for ProgrAmmable transmission and switching modular systems based on Scalable Spectrum/space aggregation for future aglle high capacity metrO Networks**
Project acronym	**PASSION**
Grant number	**780326**
Funding scheme	**Research and Innovation Action - RIA**
Project call	**H2020-ICT-30-2017 Photonics KET 2017 Scope i. Application driven core photonic technology developments**
Work Package	**WP5**
Lead Partner	**SMO**
Contributing Partner(s)	**POLIMI, CTTC, TUE, OPSYS, EFP, TID, NICT, ETRI, CHEM**
Nature	**R (report)**
Dissemination level	**PU (Public)**
Contractual delivery date	**31/05/2021**
Actual delivery date	**31/05/2021**
Version	**1.0**

History of changes

Version	Date	Comments	Main Authors
0.0	03/05/2021	ToC	G. Parladori (SMO)
0.1	20/05/2021	16X16 POLYMER MATRIX	Seo young Lee (ETRI)
0.2	24/05/2021	First draft	G. Parladori (SMO), P. Parolari, P. Boffi (PoliMI)
0.3	26/05/2021	CTTC and TUE Testbed & Experiments	M.Svaluto, R. Martinez (CTTC), N. Tessema (TUE)
0.4	29/05/2021	Quality review	POLIMI
1.0	31/05/2021	Final Version	G. Parladori (SMO), P. Parolari, P. Boffi (PoliMI)

Disclaimer

This document contains confidential information in the form of the PASSION project findings, work and products and its use is strictly regulated by the PASSION Consortium Agreement and by Contract no. 780326.

Neither the PASSION Consortium nor any of its officers, employees or agents shall be responsible or liable in negligence or otherwise howsoever in respect of any inaccuracy or omission herein.

The contents of this document are the sole responsibility of the PASSION consortium and can in no way be taken to reflect the views of the European Union.

TABLE OF CONTENTS

PHOTONICS PUBLIC PRIVATE PARTNERSHIP

TABLE OF FIGURES

PASSION

EXECUTIVE SUMMARY

Starting from the achievements of the technological WPs, in this deliverable we report about the project testbeds, describing the physical infrastructure, the preliminary activity needed to integrate the subsystems provided by the project partners and the experiments carried out at each location.

The different maturity level reached by the components and devices developed by the project and described in the deliverable D5.3, needed to invest additional activity to integrate all the functionality in a single testbed. Mechanical integration, controller boards, low lever software drivers, interface adapter, have been developed with this scope. The partners have provided a lot of work and investments, sometime exceeding the scope of the project.

PASSION developed four main testbeds, where it was possible to show the integration of the developed subsystems, namely VCSEL-based transmitter, parallel coherent receiver and switching/aggregation node. CTTC testbed was in charge of collecting the project technological achievements over a reconfigurable metro testbed, while POLIMI, NICT and TUE testbeds were targeted to support partial integration in order to overcome the issue of transferring physical devices and apparata from one site to the other. This choice helps a lot to overcome the constraint introduced by pandemic situation allowing to progress with the planned activities, even if sometime some compromises were needed.

POLIMI testbed was mainly devoted to the transmission aspects providing and extensive analysis of all the propagation impairments and limitations. NICT was mainly involved in the evaluation related to the capabilities of the exploitation of multicore fibres to increase the total transported capacity. Finally, TUE testbed was fully devoted to characterize and test the add/drop/switching subsystems. In CTTC ADRENALINE testbed the VCSEL-based S-BVT adopting integrated coherent detection was demonstrated over different connectivity scenarios. Due the pandemic situation some of the planned joint test activities has to be reshaped, integrating anyway the PASSION achievements in a SDN-managed programmable infrastructure, enabling advanced flexible features for maximizing the transported capacity and validating the PASSION technologies in the CTTC lab-trial.

1 INTRODUCTION

PASSION project aims at developing challenging photonic technologies for the next generation high-capacity optical metro network. Additional activities were planned to address the management aspects of all the innovations introduced by the project (i.e. huge bandwidth, fast configurability, flexibility, etc.). This in line with the introduction of new network paradigms such as software defined networking/ network function virtualization (SDN/NFV), disaggregation and edge computing.

In order to give evidence of the main achievements along the project execution WP5 has worked in close collaboration with other technological WPs to identify, design and disseminate a set of demonstrators representing the key steps of the project. The maturity level reached by the different building blocks constituting the innovative PASSION technological platform supporting the future metro network is at the moment not completely homogenous: so, a realistic view of the PASSION technology impact on future network infrastructure has been provided.

The deliverable is structured as follows: (i) Chapter 2 briefly summarizes the specific developments carried out by each technological WPs (i.e. WP3, WP4 and WP5), aimed at supporting the demonstration activity; (ii) in the next Chapters demonstration setups are described, and integration and test activities are reported, to demonstrate the operation of the PASSION achievements in a SDN-managed programmable infrastructure, enabling advanced flexible features for maximizing the transported capacity and validating the PASSION technologies in a relevant metro lab-trial.

2 WP DEVELOPMENTS

This chapter summarises the major achievements of the technology WPs, aimed at supporting the final test setup and demonstration activities.

WP3 was in charge of the transmission technology development. The fundamental target of the activity was the realization of a 2-Tb/s integrated photonic device incorporating 40 transmission channels based on high performance VCSEL technology provided by VERT. The device includes VCSEL drivers, selected by an external supplier, InP vertical cavity surface emitting lasers (VCSELs), SiPh arrayed waveguide gratings (AWG), electrical interposer. The integration is very challenging and requires a strong technical capability to manipulate ad assembling all the constituting parts. Many intermediate test and verification activities were carried out in order to monitor all the development steps. Furthermore, VTT invested additional effort in order to introduce a basic evaluation board, to anticipate and address all possible issues related to the use and the test of the 2-T/b transmitter chip. The evaluation board hosts one transmitter chip and provides point-to-point I2C connectivity to control all the 40 drivers with a PC equipped with a Host Adapter I2C controller (we use Total Phase - Aardvark I2C/SPI). Furthermore, VTT and SMO organized many coordination meetings to transfer all the needed chip requirements in view of the final integration of transmitter chip in the evaluation board integrated in an industry standard sub-rack (I.e. SMO LM-1 product line).

In WP4 ETRI spent effort to build a test environment around 16x16 polymer based spatial switch. More specifically, on top of a mechanical support small control board has been developed with the purpose to control the device. Further effort was spent by SMO, to provide a mechanical integration in a 300mm ETSI Standard sub rack of this device, and by CTTC to integrate the SW controller with the SDN framework. TUE provided solutions to manage the switch chipset (i.e. 4ch. 1xWSS,

2x4MCS and 10xWBL). In particular a field-programmable gate array (FPGA) based electronic controller board was developed. Software (SW) modules include low-level driver and dedicated application programming interface (API) enabling an easy integration of the node in a Standard environment, based on OpenRoadm specification (Open ROADM MSA - Home). EFP integrated two coherent receivers and related controller in a single mechanical assembly.

Further specific integration activities have been developed in WP5, as reported in deliverable D5.3. It should be highlighted the manufacturing of a transmitter board integrated on a 300mm ETSI Standard sub-rack, the mechanical integration of the spatial switch and the associated SW development needed to integrate physical devices in a SDN controlled infrastructure.

3 TESTBED @POLIMI

3.1 TESTBED DESCRIPTION

The POLIMI testbed, allows to experimentally evaluate data plane aspects of dense wavelength division multiplexing (DWDM) Metro/Core networks. In particular propagation impairments up to 2000 km (500 km SSMF) of Erbium-doped fibre amplifier (EDFA)- amplified link in C band can be evaluated. Moreover, the propagation in a spatial division multiplexing (SDM) link of up to 21 km in a 7-core multicore fibre (MCF) can be tested (for further details on SDM activity refer to Section 5). The assessment of the performance of optical links based on multicarrier modulation technology and in particular of discrete multitone (DMT) modulation, is obtained exploiting offline processing. The demonstration of the PASSION technology performance in presence of multichannel propagation down to 25 GHz spacing, characterizing the super-module VCSEL based S-BVT architecture is achieved in presence of coherent reception. The support of optical links crossing HL4 to HL3-HL2/1 nodes is demonstrated by the use of arrayed waveguide gratings (AWGs) and optical processors mimicking wavelength selective switch (WSS) devices.

3.1.1 Experimental setup

In particular Figure 1 shows the schematic of the actually employed testbed. The top row presents the envisioned PASSION network architecture including one HL4 node and two equivalent HL3 (2/1) nodes. The detailed experimental setup exploited to assess the capabilities of the PASSION technology is reported in the bottom row. Specifically, the SBV-T transmitter front-end includes a 15-GHz VERT VCSEL wire-bonded to a single-channel IDT driver HXT14100 which provides both the bias and the modulation currents and that can be piloted by the I²C interface, as described in D3.2. The VCSEL is directly modulated (DM) by a DMT signal generated by a MICRAM 100-GS/s digital-to-analog converter (DAC10002) with 35-GHz electrical bandwidth and 6 bits vertical resolution. The off-line adaptive digital signal processing (DSP) calculates by Matlab® and provides the DMT signal, which is composed of 256 sub-carriers in 20-GHz range; a cyclic prefix (CP) of about 2.1% of the symbol length is also added. The tested VCSEL emitting wavelength is 1533.5 nm, while its measured linewidth is about 5 MHz. The bias current is set at 9 mA, while the modulation depth is fixed at 8 mA in order to limit the frequency chirp insurgence and reduce the penalty due to single sideband (SSB) filtering.
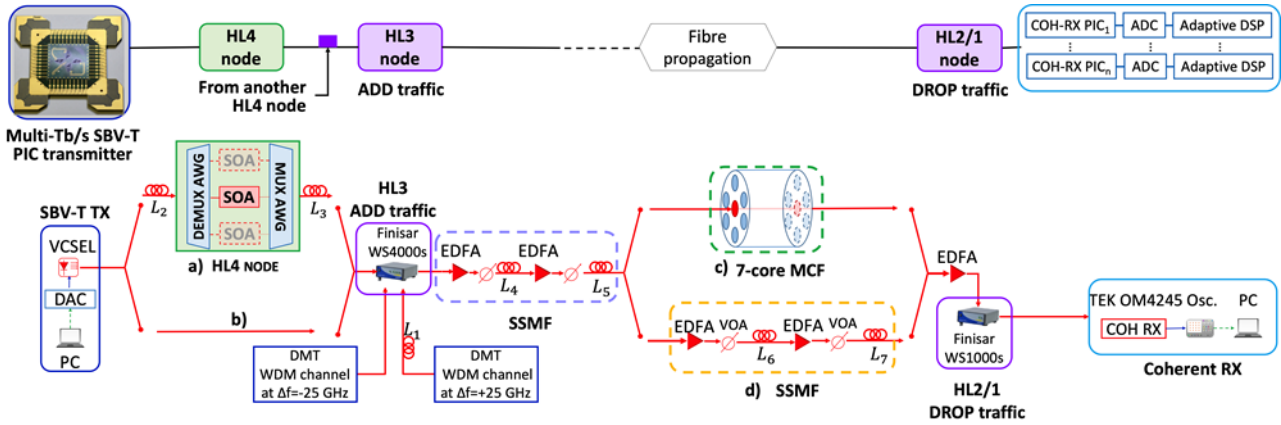
Figure 1 PASSION network architecture (top) and experimental setup (bottom) of POLIMI testbed.

At the first HL3 node another S-BVT transmitter generates the adjacent channels at ± 25 GHz from the channel under test (CUT) by modulating two 100-kHz tuneable lasers by two 25-GHz Mach-Zehnder intensity modulators. The electrical DMT signals of the adjacent channels are generated by a second DAC (DAC10002) and, in order to decorrelate the patterns of the adjacent channels, a suitable 3-km long SSMF spool has been used (indicated as L_1 in Figure 1).

The VCSEL based SBV-T output then can be: *a)* connected to a HL4 node, emulated by two 100-GHz spacing AWGs with a semiconductor optical amplifier (SOA) acting as a wavelength blocker; *b)* connected to the add-stage of the HL3 node emulated by a Finisar Waveshaper 4000s which also performs the 25-GHz spaced multiplexing (as detailed below). The optical power at the VCSEL output is -2 dBm. Considering *path a)*, the optical signal propagates in two SSMF spans of $L_2 = 9\ km$ and $L_3 = 6\ km$ before and after the HL4 crossing, respectively. The employed SOA is a 500-µm Optospeed 1550MRI/P device, which acts as a wavelength blocker reproducing the HL4 node architecture developed in WP4 and detailed in D4.3. Examples of SOA gain curves and OSNR behaviour are detailed in deliverable D5.3. The optical power at the SOA input is -10.5 dBm due to fibre and AWG losses; a SOA bias current of 200 mA has been chosen to recover the losses of the whole HL4 link while preventing the detrimental effects of SOA gain saturation described in Deliverable D5.3. At the HL4 network level the exploited channel spacing is 50-GHz and the optical signal maintains a DSB spectrum. Successively, the transmitted signal reaches the HL3 node, as mentioned before, a Finisar Waveshaper 4000s, performs the add-stage mimicking the transfer function of a 25-GHz standard WSS and performing the single sideband filtering operation thanks to 8-GHz detuning with respect to the CUT. At this stage the other two DMT channels are added after undergoing SSB filtering through the WS4000s multiplexer. The generated single-polarization optical signal is then amplified by an EDFA and propagates in two SSMF spools (indicated as L_4 and L_5 in the figure corresponding to 50 km and 54.5 km, respectively) with different launch powers. After 100-km SSMF propagation, the 3 channels can be routed to: *c)* a 3-km 7-core multicore fibre (provided by NICT) or to *d)* another SSMF link composed by L_6 and L_7 spans, targeting a maximum reach of about 200 km. A detailed list of fibre spools length is reported in Table 1. In case of MCF propagation, two different paths have been tested: 1) a single pass through the central core. In this condition, the optical signal is split before the MCF and then sent directly to the central core (CUT) or sent to a 20-dBm EDFA. After the EDFA, a 1x8 splitter is inserted in order to fill all the other cores by replicas of the 3 channels under test. Suitable fibre spools are inserted at the output of the 1x8 splitter before the lateral core inputs in order to decorrelate the channels inside the different cores both in pattern and in linewidth. 2) a several "pass-through" of the MCF by propagating serially in each core with the same 3 channels under test. In this second option, the 3 channels propagate firstly in core 1 to

enter then in core 2 and so on up to core 7. The total propagation length becomes 21 km, the optical signals in the different cores are naturally decorrelated thanks to both the MCF length and the VCSEL linewidth, thus taking into account also inter-core crosstalk impact.

Table 1. SSMF lengths

SSMF spool	Length [km]
L1	3
L2	9
L3	6
L4	54.5
L5	53.5
L6	50.9
L7	50

Finally, the CUT is selected by a Finisar WS1000s programmable filter, which mimics the HL2/1 drop stage transfer function. Then, the signal is detected by a Tektronix coherent receiver OM4245 with 45-GHz bandwidth. The local oscillator (LO) is a tuneable 100-kHz laser with +14.5 dBm optical power. The in-phase/quadrature (I/Q) signals are acquired by a Tektronix real-time oscilloscope with 8-bits vertical resolution, 100-GS/s and 33-GHz electrical bandwidth respectively. The off-line adaptive DSP performs optimal bit and power loadings (BL/PL) using Chow's algorithm assigning the appropriate bit order at each subcarrier during the mapping procedure. The adaptive DSP allows to finely tailor the spectrum with a granularity of tens of MHz, depending on the number of adopted DMT subcarriers, allowing also MAN functionalities such as multi-flow generation, slice-ability, adaptability to traffic and reach. In the experimented case, the resulting granularity is about 78 MHz. The performance of the system is evaluated in terms of capacity achievable for a target BER of $4.62 \cdot 10^{-3}$ (consistent with the use of a 7% overhead HD-FEC). The employment of non-linear Volterra Equalization (NL VE) can be also envisioned to compensate for the nonlinear impairments induced during the fibre propagation over hundreds of kilometres in presence of 25-GHz spaced channels, and also to adjust the distortions introduced by the DM VCSEL source, the DMT modulation itself, the RF commercial driver tailored for pulse amplitude modulation (PAM), and all the other electrical devices and components employed at the transmitter (TX) and receiver (RX) for the system implementation.

3.2 EXPERIMENTAL VALIDATION AND EVALUATION

The performance of the CUT in terms of capacities achievable after different propagation lengths for several system configurations are shown in Figure 2. In particular, the optimal launch power for 100-km SSMF propagation and beyond is close to 3 dBm in case of single-channel transmission (blue full circles), while in case of multichannel propagation (orange full squares) it is 5 dBm, corresponding to a power per channel around 0 dBm. The optimal condition is obtained for the same optical powers also when exploiting the Volterra equalization (green full triangles). Of course, an increase in the capacity is gained by applying the NL equalization, with a percentage improvement of more than 24% for longer propagation distances. The capacities achieved in the multichannel condition after 200-km SSMF propagation, in fact, are around 53.5 Gb/s and 43 Gb/s with and without VE, respectively. The reduction in the allowed capacity in function of the propagation length is due

both to the increase of fibre NLs and the simultaneous decrease of the optical signal to noise ratio (OSNR) achievable at the receiver, which is lowered to 34 dB after 200-km SSMF propagation.
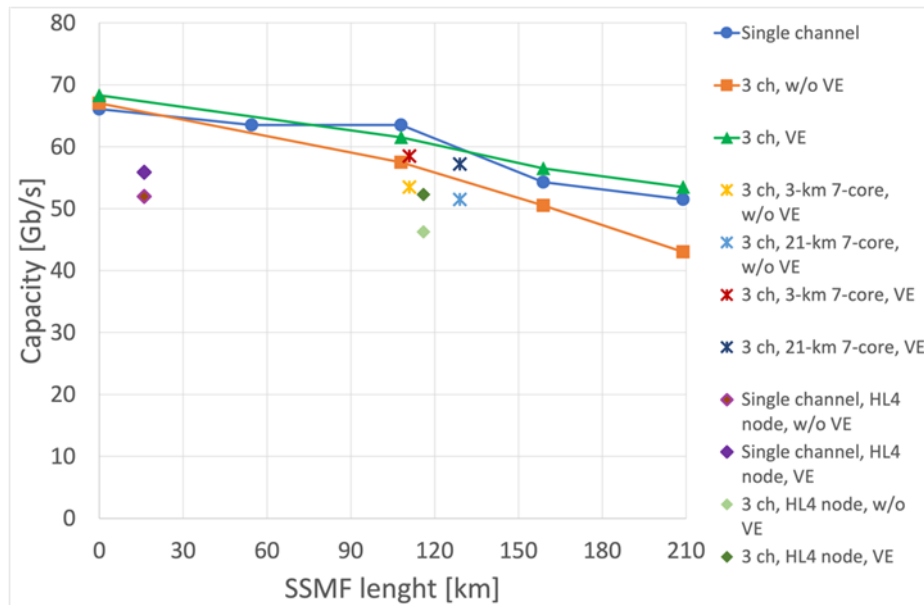

Figure 2. Per VCSEL flow capacity as a function of propagation distance with and without VE. Full symbols for SSMF only links, asterisks for hybrid SSMF and MCF links, diamonds for multi-hop HL4-HL2/1 links.

The introduction of the MCF after 100-km SSMF propagation seems to not induce any severe penalty to the system performance. In particular, the achieved capacities after 3-km and 21-km MCF propagation show a limited reduction with respect the SSMF-propagation-only curve. The faint difference with respect to the reference curves is due to a decrease of the OSNR at the receiver, which is slightly reduced by the presence of additional EDFAs in the MCF path. No additional penalties due to core interference can be noticed, thanks to the low crosstalk coefficient of the employed MCF and to the limited propagation distance.

On the other hand, the presence of the HL4 node impacts on channel performance in terms of achievable capacity. In particular, a reduction of about 14% can be noticed after 16-km propagation, while after 116 km the capacity faces a 12% drop with respect to the reference configuration without the HL4 node. This performance decrease is caused by the reduction of the OSNR at the receiver end depending on the presence of the specific SOA device employed in the testbed. The achievable OSNR after 116-km propagation and HL4 node, in fact, is close to 35 dB, similarly to the OSNR measured after 200 km in the reference condition. Since noise is detrimental to VE effectiveness, also the presence of NL equalization doesn't permit to achieve a strong capacity gain, maintaining the same percentage reduction with respect to its reference configuration. Anyway, VE removes most of NL impairments, permitting to reach more than 50 Gb/s also in presence of the HL4 node.

Table 2 summarizes the measured capacities for different system configurations when the channel under test passes through the HL4 node and the equalization is activated. The maximum reference capacity achievable with 25-GHz SSB modulation in back to back (BTB) condition is 68.3 Gb/s. The introduction of the two 100-GHz AWGs forming the HL4 node results in a capacity reduction of 4 Gb/s, owing to the increased losses and to a slight filtering effect, which impacts on the subcarriers at the high-frequency edge. The single-channel capacity is further diminished to 55.9 Gb/s in presence of the SOA, which lowers the OSNR to 38 dB. The second HL3 node, emulated by a 25-GHz bandwidth WSS, cause a tight filtering of the optical spectrum, limiting the achievable capacity

to 54 Gb/s. At last, a capacity of 52.3 Gb/s can be achieved in presence of three 25-GHz spaced channels in a multi-hop configuration constituted of an HL4 node, two HL3 aggregators, and an overall 116-km SSMF propagation. The NL VE reduces the penalty to 1.7 Gb/s with respect to 16-km single-channel propagation and to only 200 Mb/s with respect to 116-km single-channel propagation. [Rapis21]

Table 2 Achievable capacities for different system configurations in presence of HL4 node and Volterra equalization.

Distance	Configuration	Capacity
BTB	1 WSS (DEMUX)	68.3 Gb/s
	2 HL4 AWG, w/o SOA, 1 WSS	64.5 Gb/s
16 km	2 HL4 AWG, w/o SOA, 1 WSS	62.5 Gb/s
	HL4 node, 1 WSS	55.9 Gb/s
	HL4 node, 2 WSSs	54 Gb/s
116 km	Single channel	52.5 Gb/s
	3 25-GHz spaced channels	52.3 Gb/s

PASSION S-BVT technology has been demonstrated in POLIMI testbed with multi-channel propagation with 25 GHz spacing up to 200 km SSMF propagation at 50 Gb/s per VCSEL using DMT direct modulation and off- line adaptive DSP. More than 100 km can be reached with multi-hop HL4-HL2/1 paths with PASSION node emulation and MCF propagation providing in case of PASSION module an overall 2-Tb/s capacity.

4 TESTBED @TUE

4.1 TESTBED DESCRIPTION

TUE has built a test bed for evaluating on-chip switching operation realized for PASSION switching node. Specifically, the two type of switches i.e. WSS and multicast switch (MCS) have been realized. Both monolithically integrated InP and hybrid integrated SiPh/InP switches are designed, fabricated, and integrated with the optical subsystem. Figure 3 shows the test bed for fibre coupled on-chip switching. The photonic integrated circuit (PIC) switches are wire-bonded onto a printed circuit board (PCB) and are mounted on a chip holder as can be seen in Figure 3. Lensed fibres with a mode field diameter of 2.5 μm are mounted on a 3-axis alignment stage and are used to efficiently couple light in/out of the PIC. A current controller is used to inject current onto the SOAs. EDFAs are optionally integrated to compensate any excess losses. In this test bed, insertion loss of the on-chip switch, transmission spectrum and as well as bit error rate are measured. A BERT is used to generate data to be modulated on a Mach-Zehnder modulator. After transmission through the on-chip switch the optical signal for a given wavelength channel is detected by a photodiode (PD). The selection of the measured channel is done by a tuneable filter. The bit error rate is generated by BERT system by comparing the transmitted data and the received/detected data.
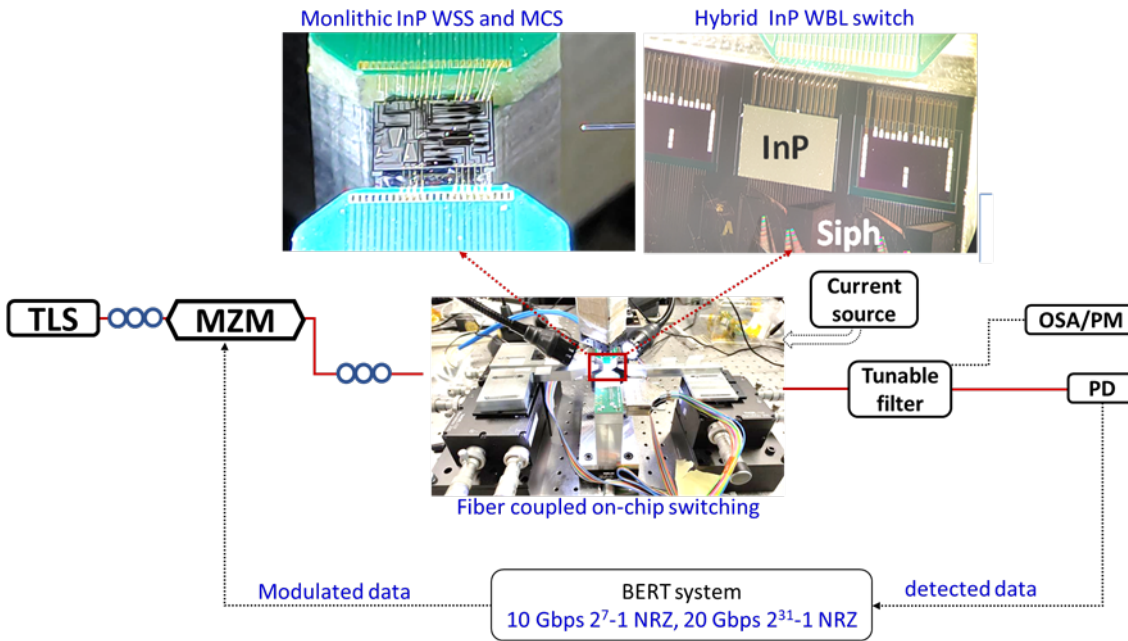
PHOTONICS PUBLIC PRIVATE PARTNERSHIP

Figure 3.Testbed for fiber-coupled on-chip switching on Monolithic InP and Hybrid SiPh/InP platform

## 4.2 DATA TRANSMISSION AT 10 GBPS AND 20 GBPS THROUGH THE HYBRID WBL

A tuneable laser source is used to generate light for wavelengths corresponding to the channels of the wavelength blocker (WBL). Lensed fibres are used to couple light in/out of the hybrid WBL switch. The input optical modulated data was boosted to 17 dBm to compensate the losses in hybrid WBL. After transmission through the WBL, the output signal is variably attenuated before being input to the receiver. A 2^7-1 NRZ 10Gbps data is externally modulated and transmitted through the hybrid WBL switch and detected at the receiver. Figure 4 shows the BER measurements of five functioning channels of WBL Ch1, Ch3, Ch6, Ch7 and Ch8 at 10Gbps 27-1 PRBS NRZ data. Error free transmission is obtained with power penalties ranging from 0.3 dB to 1.5 dB. Clearly opened eye diagrams of the five channels are obtained as shown in Figure 4(a).

After the transmission through WBL, a second preamplifier is used to reach the sensitivity of the 20Gbps receiver. A tunable filter with 3 dB bandwidth of 200 GHz is used before the receiver. Error free transmission is achieved for Ch1, Ch3, Ch6, Ch7, and Ch8 as shown in Figure 4 (b) and Table.3. The penalties range for 0.7 dB in case of Ch3 and 2.8 dB in case of Ch8 at BER of 1E-9. The current of the SOA for each channel is optimized to minimize power penalties. These successful data transmissions performed on the first proof-of-concept modularly designed hybrid WBL verify its feasibility to be used in high capacity metro-core switching node where capacity can be scaled by adding new modules in a pay-as-you-grow manner. This first trial assembly process is followed by on-going efforts to reduce excess hybrid coupling losses via optimization of the flip-chip assembly process, the use of on-chip spot-size converter to relax tight alignment tolerances, and by employing angled waveguides at the facets to reduce back reflection.
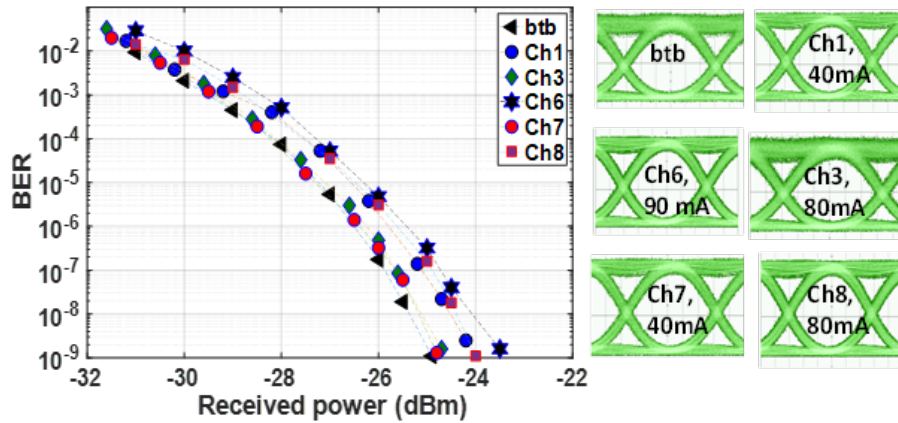
a)
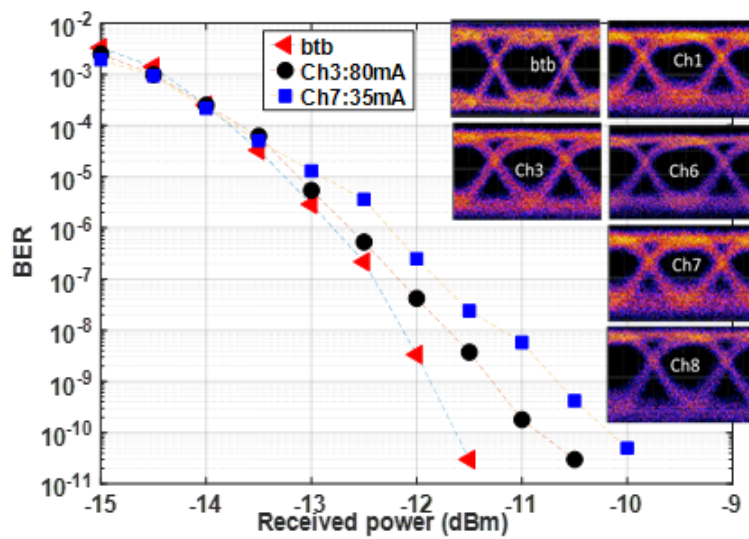
b)

Figure 4.BER vs received power at 10 Gbps NRZ (b) BER vs received power at 20 Gbps NRZ

Table 3 POWER PENALTY @ BER 1E-9 FOR 20 GBPS TRANSMISSION

Channel	Ch1	Ch3	Ch6	Ch7	Ch8
Penalty (dB) at 1E-9	1.3	0.7	2	1.4	2.8
Current (mA) of SOA	35	80	90	35	60

5 TESTBED @NICT

Due to COVID-19 emergency situation, exchange of researchers and equipment with Japan has been very difficult. Nevertheless, in order to evaluate the PASSION technology performance in a SDM scenario POLIMI and NICT discussed and developed a set of experimental measurements at POLIMI premises using NICT 7-core MCF.

5.1 LAB DESCRIPTION

NICT can provide a multicore-fibre network: its testbed is equipped to explore transmission over various space division multiplexed fibres (Figure 5).
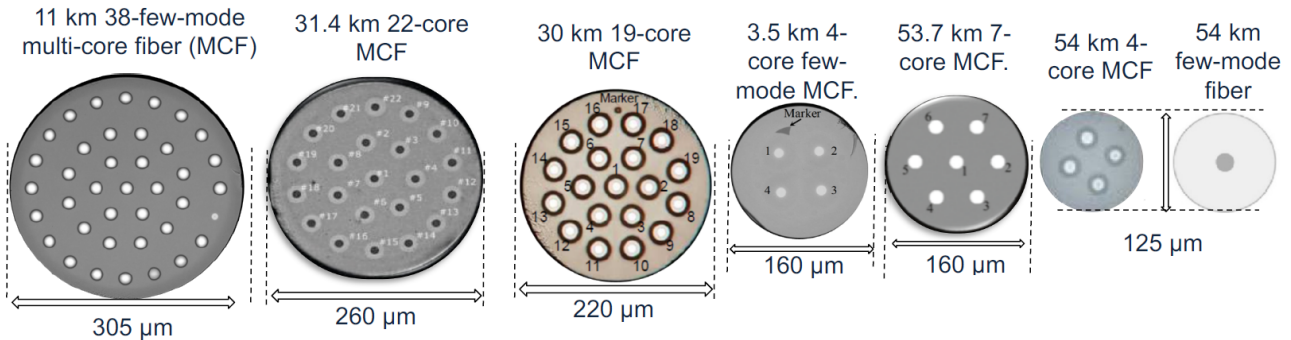
Figure 5. Available multicore fibre

Furthermore, it is also possible to use 45 km of deployed fibre link from NICT (West Tokyo) to Downtown Tokyo (Figure 6) and inline fibre test-bet up to 10.000 km

Figure 6. Available deployed Fibre in Tokyo Area

Lab equipment includes (Figure 7):

- various digital sampling scopes (up 160 GS/s) for reception and offline processing, 80Gs/s scope with 12 or more channels for SDM or simultaneous multi-channel reception
- amplifiers and components for transmission in C-, L- and, if needed, S- band
- 64 x 64 Polatis switch and 44 x 44 Fujitsu switch (emulate various node/network topologies with MCFs or SMFs)
- Multi-core fibre switching devices also available
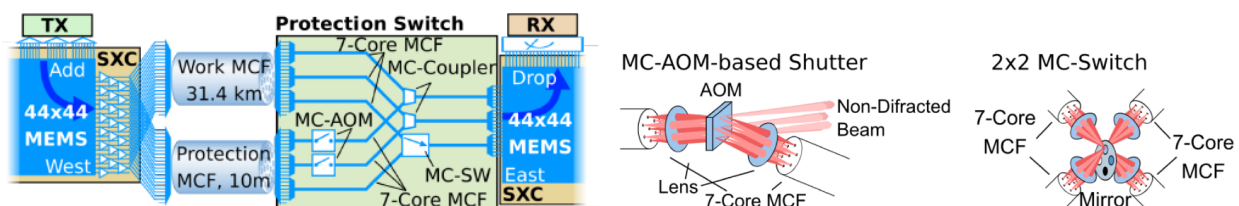
Figure 7. Available Switching Devices

5.1 JOINT EXPERIMENT ON IMPAIRMENTS DUE TO INTER-CORE CROSSTALK DYNAMICS IN MCF LINK WITH PASSION TRANSMISSION TECHNOLOGY: DESCRIPTION AND TEST RESULTS

PASSION transmission technology exploiting multiple DM VCSELs and multicarrier modulation represents a peculiarity for SDM systems usually relying on single carrier WDM signals. In fact, the DMT signals are characterized by a high carrier to signal power ratio (CSPR), which can lead to strong inter-core crosstalk (ICXT) fluctuations over time. Moreover, the time-dependent impairments induced by the beating between different optical sources feeding the fibre cores must be studied. PASSION transmission technology exploitation represents thus an application scenario of MCF systems, using independent directly modulated DMT sources on each core with the same nominal wavelength but with time-varying frequency shifts, due to laser frequency wandering.
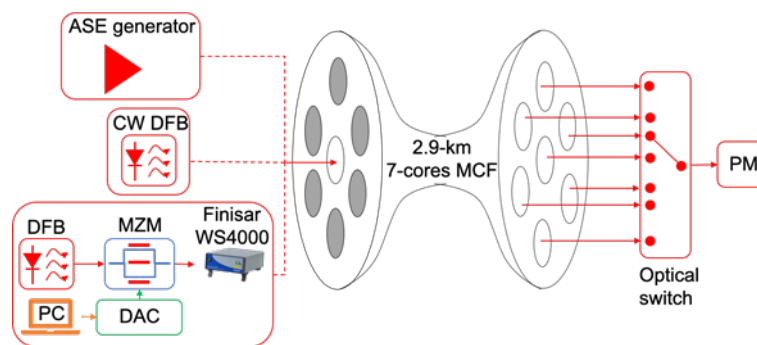
Figure 8. Experimental setup for STAXT measurement.

In order to evaluate this scenario, we employed the experimental setup shown in Figure 8 suitable for analysing the dynamic crosstalk. We used a 2.9 km homogeneous single-mode 7-core MCF, where each fibre core has a step-index profile with a cladding refractive index of 1.4445 and core-cladding index difference of 0.42%. Two 3D waveguide couplers acted as SDM multiplexer and demultiplexer, leading to an average loss of 4 dB per core. A crosstalk-generating signal, consisting of either amplified-spontaneous emission (ASE) noise, a CW lightwave or DMT signals with SSB or dual sideband (DSB) modulation, was injected into the central core. The DMT analysis has been performed using a externally modulated source to remove any possible impairment due to laser wandering. After demultiplexing, an optical switch was used to direct each core output sequentially to a power meter (PM). This allowed measuring the short-term average crosstalk (STAXT) every 10 seconds over a period of 16 hours.

Figure 9.Crosstalk characterization.

PASSION

Examples of STAXT profiles from the central core to one of the adjacent cores are shown in Figure 9, while the average, variance and peak-to-peak values for each configuration are reported in Table 4. As expected, the crosstalk profile is nearly constant in case of ASE noise, confirmed by the low variance and peak-to-peak variation. Conversely, strong fluctuations were observed with CW and DMT signals with maximum variance of 8.3 dB for the continuous wave (CW) l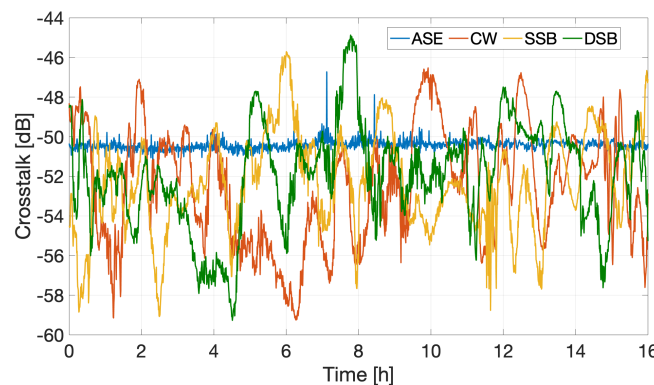aser and 14 dB peak-to-peak ratio for DSB modulation, showing that the strong carrier in high CSPR DMT signals leads to STAXT evolution resembling a CW signal.

Table 4. Crosstalk from central core to adjacent core.

	Average [dB]	Variance [dB]	Peak to peak [dB]
ASE	-50.5	0.05	0.8
CW	-51.9	8.3	12.8
SSB	-51.6	5.95	13.4
DSB	-51.2	6.7	14.4
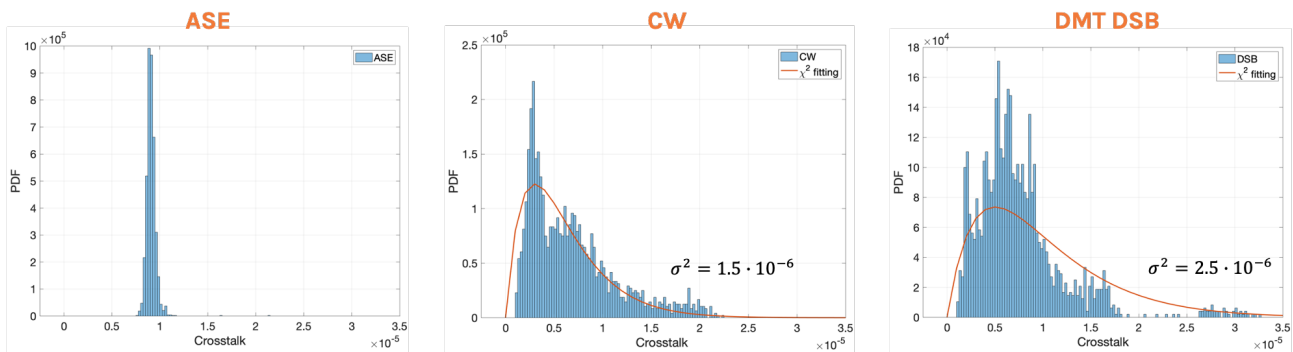
Figure 10. Histograms of STAXT for different propagating signals.

The different behaviour of the analysed signal configurations clearly appears in Figure 23, where the histograms of the STAXT contribution are reported for ASE noise, CW lightwave and DMT DSB optical signal. In particular, in case of ASE noise a narrow Gaussian-like distribution can be measured, confirming the very stable behaviour of inter-core crosstalk in such a configuration. On the other hand, CW and DMT DSB signals are characterized by χ^{2-like} distributions with two different scaling factors, reported in the insets of the respective figures. This specific behaviour is expected, since in intensity-modulated DMT signals a strong carrier arises, making them similar to a CW radiation with a superposed Gaussian perturbation. It is interesting to notice that the average STAXT in case of CW and DMT signals is lower than the correspondent one measured with ASE noise. However, owing to the χ^{2-like} profile, a wider distribution is found, leading to stronger STAXT contributions from core to core. [Gatto21].
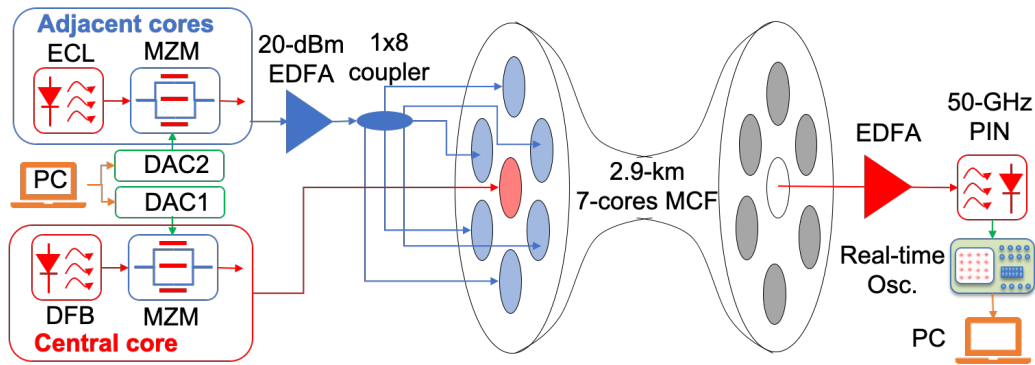
Figure 11. Experimental setup for DMT transmission performance evaluation.

Figure 11 shows the second experimental setup used to measure the performance of an optical link based on the 7-core MCF. The 7 cores carried externally-modulated DMT-based DSB optical signals generated by two different laser sources. We used a 500 kHz linewidth distributed feedback laser (DFB) to produce the signal transmitted in the central core. Similarly, we used a 300 kHz tuneable external cavity laser (ECL) to produce the signals transmitted in the outer cores. In order to emulate independent signals, SMF spans were used for temporal decorrelation with the lengths chosen to exceed to coherence length of the tuneable laser. The ECL wavelength was tuned to within few hundreds of MHz from the DFB one. The ICXT was purposely increased to emulate the behaviour of longer links by launching +6.5 dBm average power in the outer cores and -13.5 dBm in the central one. The nominal wavelength of the DFB and tuneable source was 1558 nm, while both intensity MZM had 25-GHz bandwidth. The 20-GHz DMT signal was computed offline and comprised 256 subcarriers, leading to a sub-carrier spacing of 78.125 MHz; a CP of about 2.1% of the symbol length was added for symbol synchronization and chromatic dispersion mitigation. To address the impact of ICXT fluctuations on the transmission performance, the sub-carriers were uniformly-loaded with quadrature phase-shift keyed (QPSK) modulation. In order to highlight the time-varying effect of the ICXT on the signal and its frequency-dependent behaviour, no bit- and power-loading algorithms have been applied. Since the DMT signal is composed by QPSK subcarriers, it is possible to continuously check the evolution of the SNR of each subcarrier during the measurement. Moreover, the BER value could be used as an indicator of the impact of ICXT, while in case of adaptive bit- and power-loading algorithm just the transported capacity can be observed. The electrical signals were generated by 100 GS/s digital-to-analog converters with 40-GHz electrical bandwidth and 6-bit vertical resolution. The signal from the central core was pre-amplified by an EDFA and directly detected by a 50-GHz PIN photodiode at a constant power of +10 dBm for all measurements. The signal was then digitized in a real-time oscilloscope with 8-bit vertical resolution, 100 GS/s and 33-GHz electrical bandwidth. Digital signal processing (DSP) was implemented off-line and included digital symbol synchronization, CP removal, sub-carrier phase recovery and demodulation, and BER counting. Firstly, an ICXT measurement was performed to evaluate the STAXT from the adjacent 6-cores to the central one by switching off the signal in the central core in case of DMT DSB modulation. The STAXT variation is shown in Figure 12 Figure 25, while its average, variance and peak-to-peak values are reported in Table 5. Owing to the incoherent mixing of 6 crosstalk signals with similar optical power originating from different independent cores, the cumulated STAXT variation is damped with respect to the single core situation of Figure 9 and Table 4. However, the STAXT still presents a time-varying behavior, with a peak-to-peak variation lower than 6 dB.
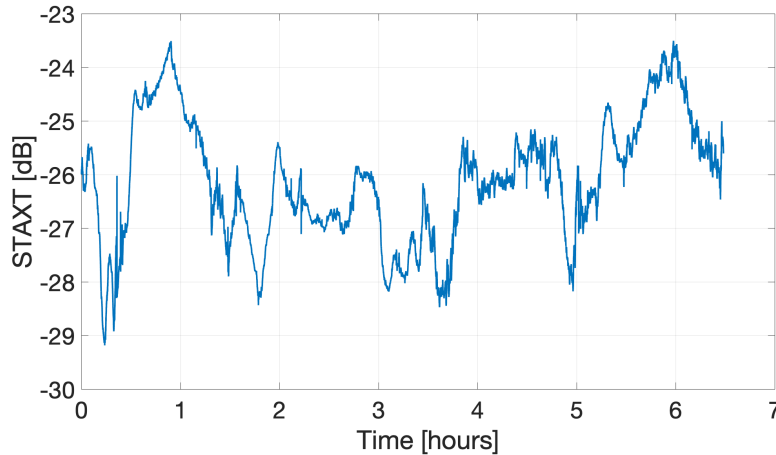
Figure 12. Cumulative STAXT on the central core

Table 5. STAXT from 6 outer cores to the central core.

	Average [dB]	Variance [dB]	Peak to peak [dB]
6-core DSB	-26	1.33	5.7

Finally, the impact of cumulated STAXT fluctuations has been analysed measuring the performance of the signal in the central core over a time period of 16 hours in terms of cumulative BER and of signal t onoise ratio (SNR) per subcarrier. Since the DMT subcarriers are uniformly-loaded by QPSK modulation, the cumulative BER can be used as a suitable indicator of the overall performance, while the SNR indicates the quality of the specific subcarrier. Figure 13 reports the evolution of the SNR curve over time. In particular, the SNR generally shows a low-pass-like profile, although a strong degradation at the frequency difference between the DFB and ECL can be observed. Owing to the presence of this beating tone, the SNR close to those positions is almost null, i.e. the subcarrier signal is drowned by the beating tone. The position of the frequency dip changes over time due to a slow oscillation of the tuneable source emission in a 2-GHz range. Moreover, some frequency patterns arise in the SNR curves, similar to modulation frequency dependent fluctuations already reported.

Table 6. Average, standard deviation and peak-to-peak values of the BER in case of all-core and single-core excitation.

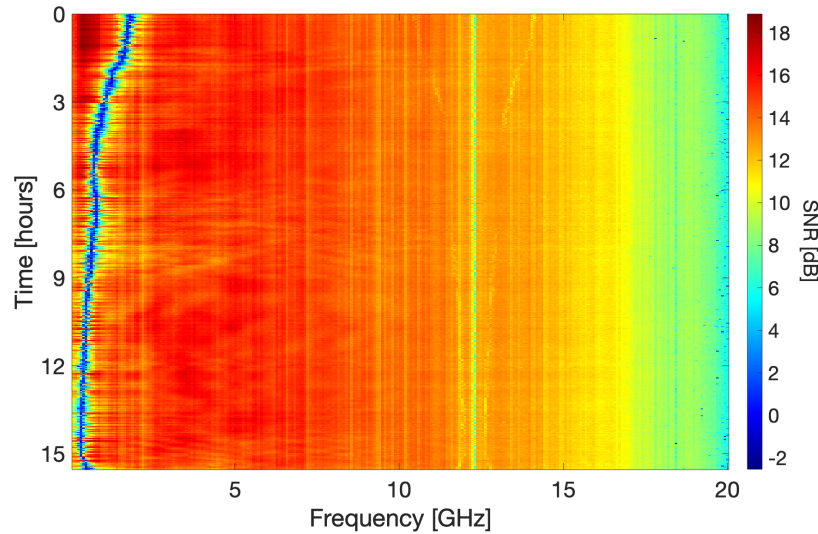|	Average	Std	Peak2peak
7 cores	$3.8 \cdot 10^{-3}$	$1.1 \cdot 10^{-3}$	$5.6 \cdot 10^{-3}$
1 core	$4.7 \cdot 10^{-4}$	$5.7 \cdot 10^{-5}$	$3 \cdot 10^{-4}$

Figure 13. Evolution of the SNR vs electrical frequency over 16 hours

The frequency patterns seem to appear in the low frequency range, while no significant variation can be noticed in the spectral region beyond 12 GHz, which seems to remain unchanged during the measurement time. Cumulative BER fluctuations are shown in Figure 14 together with the reference measurement obtained in case of single core excitation. The average, standard deviation and peak-to-peak values of the BER in case of 7-core and single-core propagation are reported in Table 6. In the single core situation, the BER curve is quite stable, with a limited drift and a negligible fluctuation over all the 16 hours, as stated by the very limited standard deviation. On the other hand, when the adjacent 6 cores are switched on, an average degradation of about a decade appears. The BER deterioration is due to both the presence of the beating tone between the two optical carriers and to a general reduction of the SNR values, owing to an incoherent crosstalk close to -25 dB. A time-dependent variation in the BER value appears, as shown by the red trend-line of Figure 14 and by the spreading of the raw BER data obtained (blue diamonds). This time-varying performance could be originated both by the crosstalk fluctuations but also by the instantaneous polarization difference between signal and interferers. In fact, since the signals are single polarization, the relative polarization states of signal and crosstalk can enhance or depress their beating at the receiver end. In order to check the polarization behaviour of the system, its evolution has been monitored during the BER acquisition using a PAT9000 polarimeter. In particular, three configurations have been analysed: a) the presence of the DMT signal alone; b) the presence of the cumulated 6-core alone; c) the simultaneous presence of DMT signal and inter-core crosstalk. The correspondent polarization evolutions are shown in Figure 15. When just the DMT signal is present, a noiseless trace can be acquired, with the state of polarization travelling on the Poincarè sphere during the 16 hours of measurement due to environmental changes and the birefringent action of the fibre. Observing the polarization of the cumulated crosstalk, instead, a very noise trace is detected, with no specific polarization drift but just a chaotic behaviour. This result is expected, since the analysed crosstalk is the sum of 6 uncorrelated contributions completely decorrelated one respect to each other thanks to the suitable fibre spans placed between the 1x8 splitter and the input of the lateral cores. Finally, the polarization evolution in case of simultaneous presence of DMT signal and crosstalk shows a well-defined trace on the sphere, even though in this case a strong noise is superposed. Anyway, no significant changes in the width of the polarization trace can be noticed, evidencing that the crosstalk variation during time doesn't induce any specific impact on the polarization apart from a general quick variation as a noise-like effect.
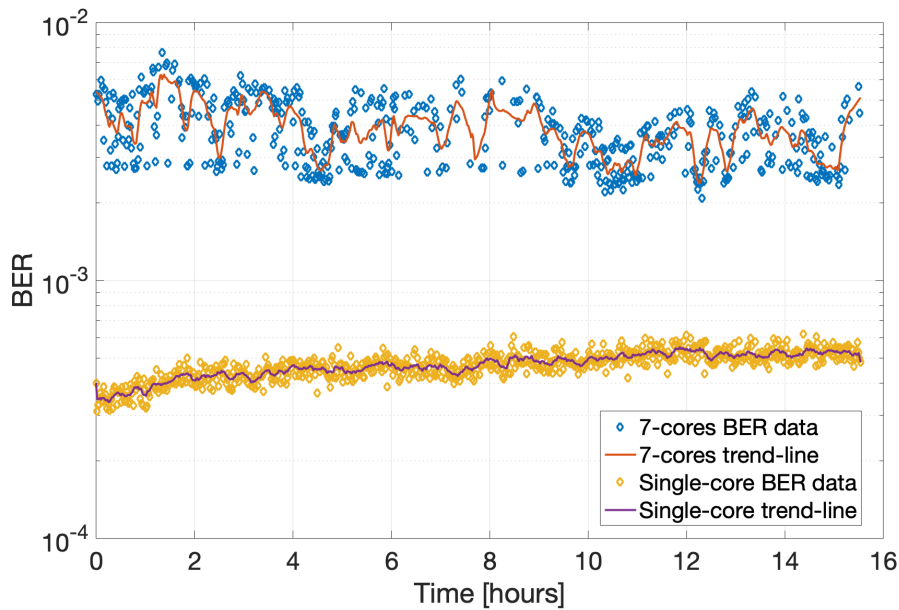
PASSION

Figure 14. BER measurements (7-cores – blue diamonds, single core – yellow diamonds) and relative trend-lines (7 cores – red line, single core – purple line).
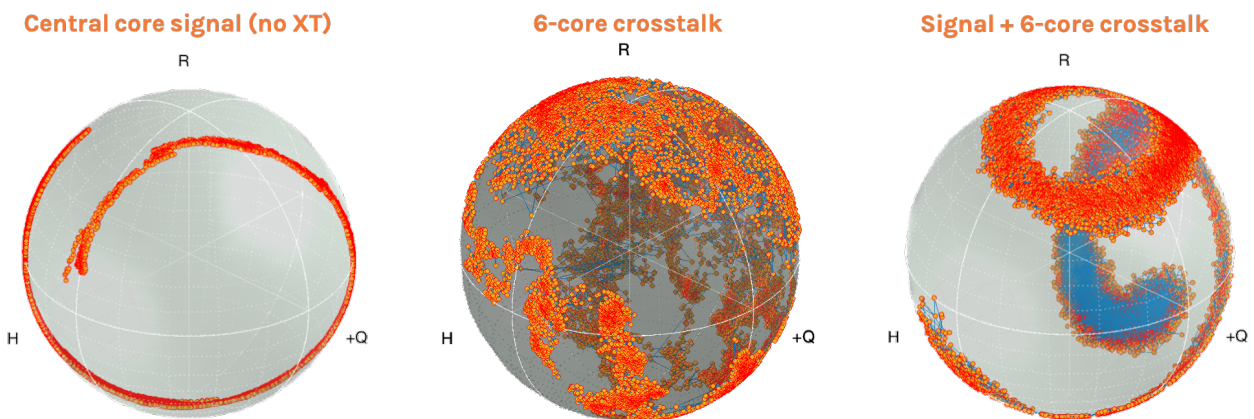
Figure 15. Polarization evolution in case of (left) DMT signal only, (center) cumulated 6-core crosstalk only and (right) DMT signal with inter-core crosstalk.

In conclusion, to analyse the SDM scenario more likely resembling PASSION transmission technology exploitation we investigated time-dependent performance impairments due to ICXT in a 7-core MCF in presence of different laser sources at the same nominal wavelength. DMT modulation, both in DSB and SSB case, is characterized by high CSPR and it induces strong ICXT fluctuations. Thanks to the experimentally chosen 20-dB power loading imbalance, ICXT levels consistent with hundreds of kilometres of MCF propagation were evaluated. Measurements showed that loading all 6 outer cores reduced the cumulative ICXT power variation on the central core. Owing to the time-varying frequency shift of the lasers, different impairments are demonstrated for each DMT subcarrier over time, depending by the sources beating.

6 TESTBED @CTTC

6.1 TESTBED DESCRIPTION

As described in D5.1, the CTTC ADRENALINE testbed®, including the EOS platform (Experimental platform for Optical OFDM System), allows to experimentally evaluate different data and control plane aspects in a heterogeneous infrastructure featuring, among other capabilities, a DWDM Metro/Core network with four optical nodes. The ADRENALINE testbed® encompasses multiple interrelated although independent components and prototypes, to offer end-to-end services, interconnecting users and applications across a wide range of heterogeneous network technologies. ADRENALINE includes a multi-technology SDN control and orchestration system handling multi-layer network infrastructure combining packet over optical switching; while, the EOS platform allows the development and assessment of optical connectivity solutions, based on multicarrier modulation (MCM) technology (either OFDM or DMT), adopting offline processing. Towards the demonstration of the PASSION network and concepts, the S-BVT architecture is based on the choice and technologies envisioned in the project (e.g., VCSEL technology and coherent reception) and the path to be considered include both the real network of the ADRENALINE testbed for spectral switching as well as the 25 km 19-core MCF for the spatial dimension assessment. Multi-hop paths are established to prove the PASSION concept and main use case(s) for the support of HL4-HL2/1 optical connectivity.
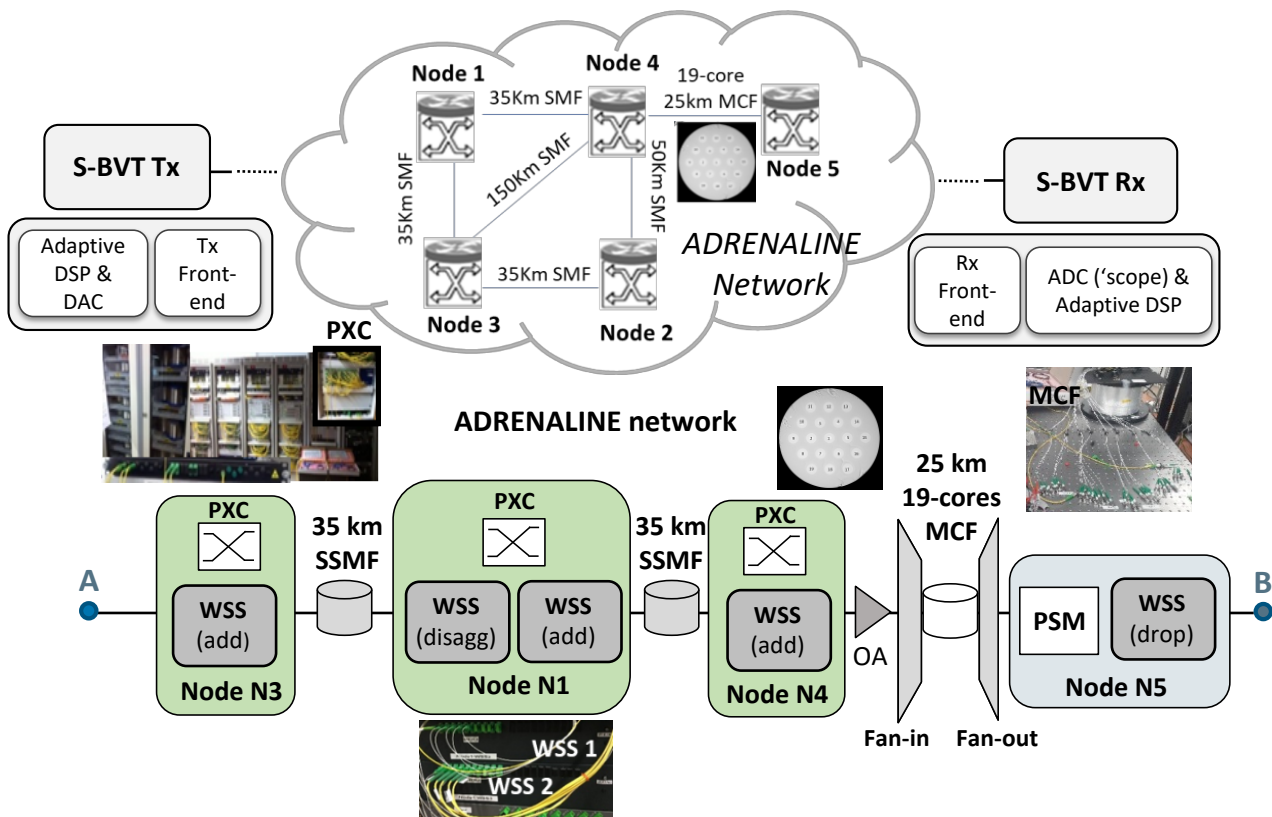

Figure 16. Testbed layout for the PASSION assessment, indicating the ADRENALINE network and (from point A to B) a possible path established over the network including the 25 km 19-core MCF. S-BVT Tx/Rx can be directly attached to point A/B or other network elements can be also included/integrated towards demonstrating the PASSION concepts and technological solutions.

The ADRENALINE network is a photonic mesh network with optical disaggregated nodes adopting WSSs and AWGs as multiplexer/demultiplexers. It consists of 4 nodes (photonic crossconnects, PXCs, and reconfigurable add-drop multiplexers, ROADMs) and amplified single mode fibre (SMF) links of 35 km, 50 km and 150 km, for a total of 600 km. It also includes a 19-core MCF with fan-in and fan-out towards the drop (destination) node. After the MCF, a photonic switch module (PSM) can be envisioned (either emulated with an optical attenuator), followed by an optical filter (to emulate a WSS) for dropping the signal towards the destination node.

In particular, for the HL4-HL2/1 path emulation, the following elements are considered:

- 2 AWGs and 1 SOA (for HL4 node emulation)
- 6 WSSs & photonic switch (PS) (HL3, HL2/1 multiple functionalities)
- 25km 19-core MCF with fan-in/fan-out
- ADRENALINE network (EDFA pre-amplified SSMF links)
- Different path can be established
- Availability of recirculating loop

6.2 INTEGRATION ACTIVITIES

Despite the difficulties due to the COVID-19 situation, the lockdown and limited access to the lab, as well as related delay and issues with components availability, integration, different activities have been conducted in order to provide the proof of PASSION concepts and envisioned metro network validation.

We have included a PSM to manage the spatial dimension and enabling spatial switching, thanks to the integration of the ETRI 16x16 polymer switch.

Due to the unavailability of the fundamental module integrating multiple VCSELs, as a contingency measure, we have integrated in the testbed different VERTILAS VCSEL samples and a laser current control system (LCCS) and developed the corresponding S-BVT Tx agent, so that the SDN controller is able to configure the VCSEL-based S-BVT flows/slices, suitably activating them.

At the receiver side, an integrated coherent receiver has been considered as benchmark towards the further integration of the EFP coherent receiver module (CRM). A tuneable laser source acting as local oscillator has been also integrated, which can be controlled by the software defined networking (SDN) controller thanks to the appropriated developed S-BVT Rx agent.

The implemented set-up allows the connection of the different integrated network elements with the ADRENALINE photonic mesh network and thus the configuration of the nodes over the established path, as shown in Figure 17.
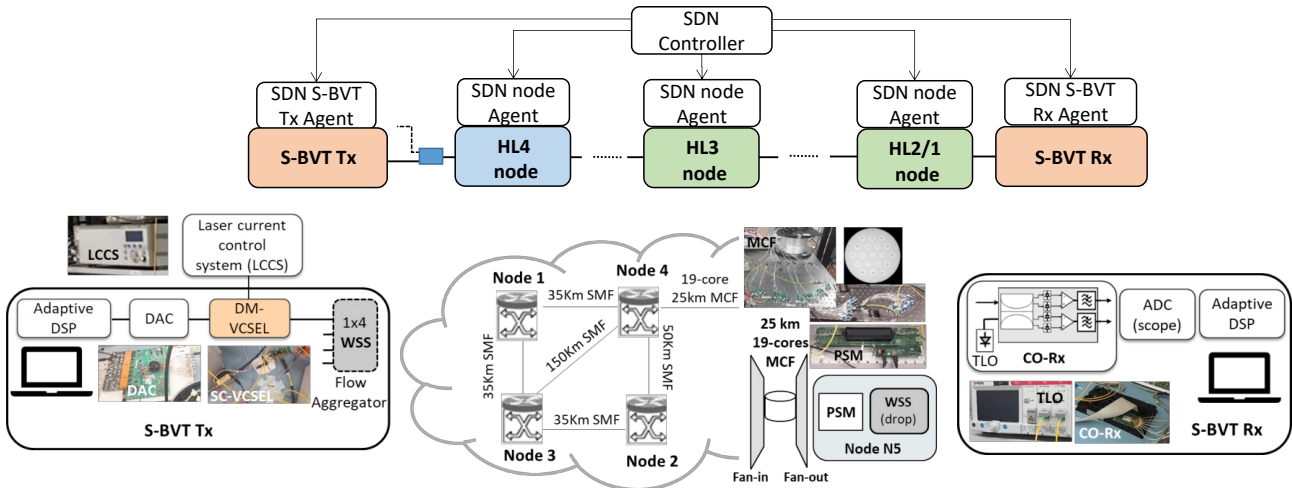
Figure 17. SDN-controlled photonic system, including the ADRENALINE network with examples of integrated elements (at S-BVT Tx/Rx and node with spectrum/space switching).

Experiment 1 – SDN-controlled photonic system architectures for MAN connectivity. Preliminary results have been obtained at an early stage of WP5 activities to demonstrate the PASSION concept for supporting large MAN connectivity [Sval20]. In this study, direct detection (DD) and coherent receiver (CO-Rx) solutions have been compared to support MAN connectivity adopting VCSEL-based S-BVT over a multi-hop (6 hops) path covering the targeted large MAN distance (160 km) between HL4 and HL2/1 nodes. The experimental assessment has been performed considering a VCSEL with bandwidth limited to 10 GHz. However, a maximum capacity beyond 35 Gb/s has been obtained in BTB thanks to the use of MCM modulation, with adaptive bandwidth up to 16 GHz, and applying pre-emphasis at the S-BVT Tx DSP. Also, it has been demonstrated that using an integrated CO-Rx module provides better performance than using a CO-Rx with discrete components and similar responsivity. Similar performance as DD can be achieved in B2B and negligible penalty is found after traversing a short (2-hop 15 km) path. In case of multi-hop connectivity traversing multiple nodes of the ADRENALINE testbed and larger path (up to 160 km), it has been shown that the best option is to adopt CO-Rx, as proposed to adopt in the framework of the proposed PASSION project, since the chromatic dispersion and chirp effects severely degrade the performance of the S-BVT architecture based on DD. Above 20 Gb/s capacity has been obtained with the 10 GHz VCSEL-based S-BVT adopting CO-Rx with discrete components.

Considering these results as a reference, we have shown that with higher bandwidth short cavity (SC) VCSELs (18 GHz) and integrated CO-Rx, higher capacity per flow can be targeted, as envisioned in the project and really promising results for the PASSION approach has been achieved. In particular, considering the 160 km 6-hop path, the numerical assessment demonstrated that the expected supported capacity per flow is higher than 40 Gb/s (considering 25 GHz granularity), resulting in a total aggregated capacity of 1.6 Tb/s activating all the 40 VCSEL flows generated at the S-BVT fundamental module. It should be taken into account that considering 25 GHz granularity, the filter narrowing effect impacts on the system performance and it could be eventually mitigated with a reduction of the modulated bandwidth for limiting the adjacent spectral channel crosstalk.

To further enhance the capacity performance of the proposed S-BVT solution towards the support of >100 Tb/s connectivity, the spatial dimension (either using a bundle of fibres or MCF) can be exploited. In the case of using MCF, the impact on the maximum supported capacity due to crosstalk effect and nonlinearities should be considered, especially for large MANs. The results over the 25 km MCF from ADRENALINE node 4 to node 5, show that the S-BVT VCSEL flow capacity without

crosstalk is higher than the one obtained in presence of the crosstalk derived from the activation of the adjacent cores [Sval1-21. For assessing large MAN connectivity, longer MCF paths are assessed in the ADRENALINE testbed implementing an optical fiber loop, showing that the capacity obtained for 25 km is halved after 200 km [Sval2-21].

The set-up including the real testbed network of the ADRENALINE testbed, the 25 km 19-core MCF and the available PASSION components has been further enhanced towards the integration of data and control plane. Different VERTILAS VCSELs have been tested and integrated to generate multiple adaptive flows/slices at the S-BVT Tx. An additional photonic switch module (ETRI 16x16 polymer switch) to manage the spatial dimension and enabling spatial switching, has been integrated after the MCF link and included in the last node as shown in Figure 17.

To demonstrate the targeted use case for the support of large 5G-supportive MAN with the proposed system solutions, the SDN-controlled system, including the VCSEL-based S-BVT with Co-Rx and the network nodes, has been considered as indicated in Figure 18.
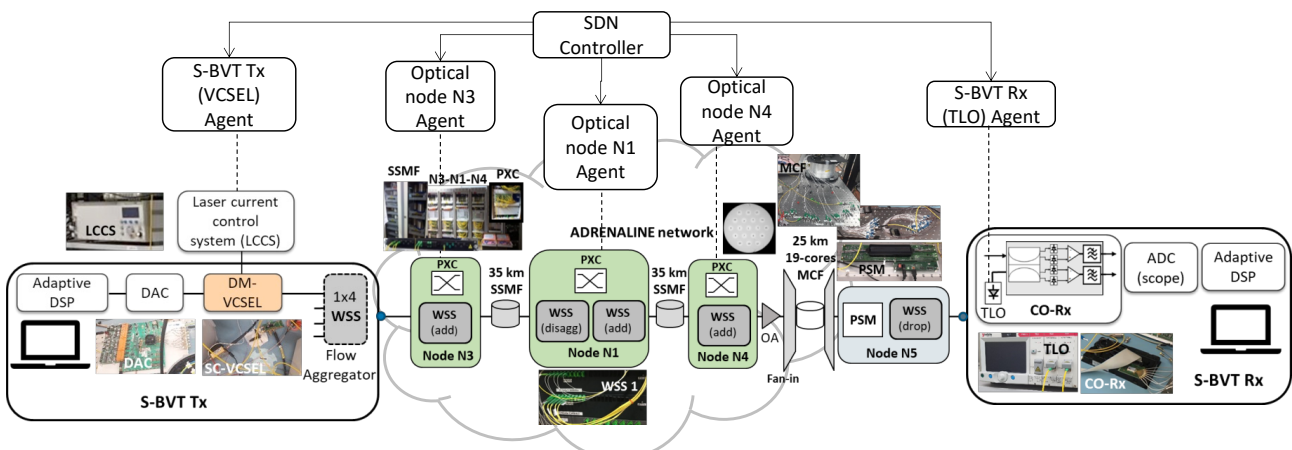

Figure 18. Schematic of the experimental demonstration of the SDN-controlled VCSEL-based photonic system for MAN connectivity.

The use of the ADRENALINE testbed network with optical disaggregated (white box) nodes has been particularly relevant to demonstrate the validity of the proposed approach in disaggregated optical network. To demonstrate the support of both the spectral and spatial dimensions at higher hierarchical level, in addition to the ADRENALINE network (links and nodes), the MCF with fan-in and fan-out and the polymer PSM have been included. The VCSEL-based S-BVT Tx is activated by a LCCS thanks to the developed corresponding S-BVT Tx agent. At the receiver side, an integrated CO-Rx with a tuneable laser source acting as LO is controlled by the SDN controller by means of the appropriated S-BVT Rx agent.

The SDN controller after selecting the resources and coordinating the establishment of the optical path over the ADRENALINE testbed network (see Figure 19), configures the underlying data plane elements. Two scenarios have been considered: 1) the 70 km optical path traversing the ADRENALINE nodes N1, N3 and 2) the ADRENALINE 70 km path, including also an additional hop and the spatial dimension handling, with the 25 km 19-core MCF and the 16x16 polymer switch module. At node N5, before the CO-Rx, a WSS is considered for dropping the optical flow.
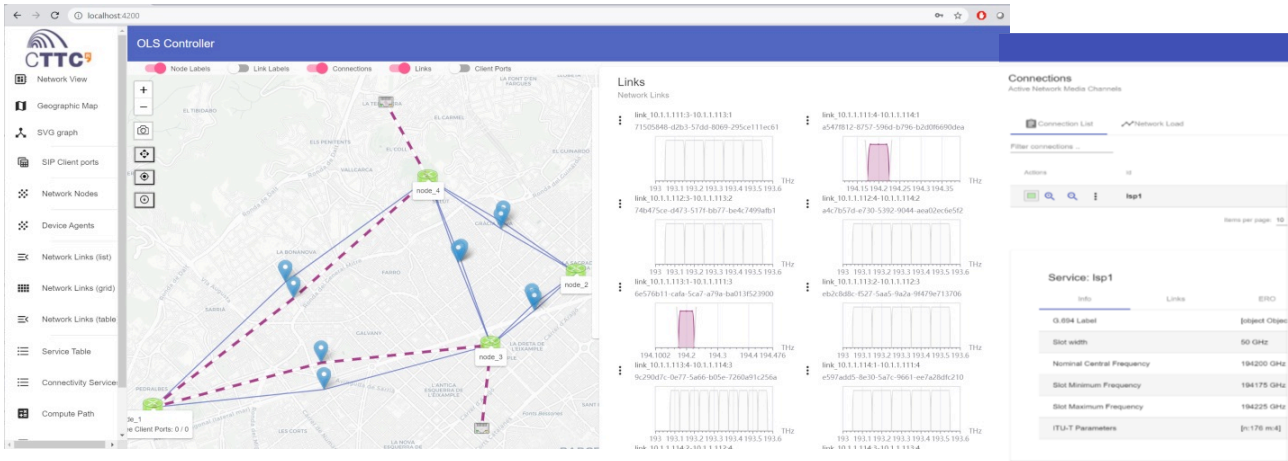
Figure 19. SDN control GUI showing the established connection over the N3-N1-N4 path (dashed line), indicating a possible deployment of the metro network in Barcelona (on the left), also the connection in terms of central frequency (at 194.200 THz, n=176) and slot width (50 GHz, m=4) are indicated.

We have demonstrated that the SDN controller is able to configure i) the VCSEL-based S-BVT flows/slices, activating/de-activating the VCSEL optical flow at the considered operating wavelength (in terms of n, being $193.1+n\cdot0.00625$ THz), ii) the traversed nodes (different granularities can be selected at the network nodes by defining the slot width as $2\cdot m\cdot6.25$ GHz), and iii) the TLO at the appropriate frequency. Successful transmission is achieved over the established path in both the scenarios, targeting 25 Gb/s flow for scenario 1 and 20 Gb/s flow for scenario 2. The SDN-controlled system for MAN connectivity demonstration will be presented in the demo zone of next OFC 2021 [Sval3-21].

An example of S-BVT Tx/Rx and node configuration at n=144 and m=4 is reported in Figure 20 [Sval-21].
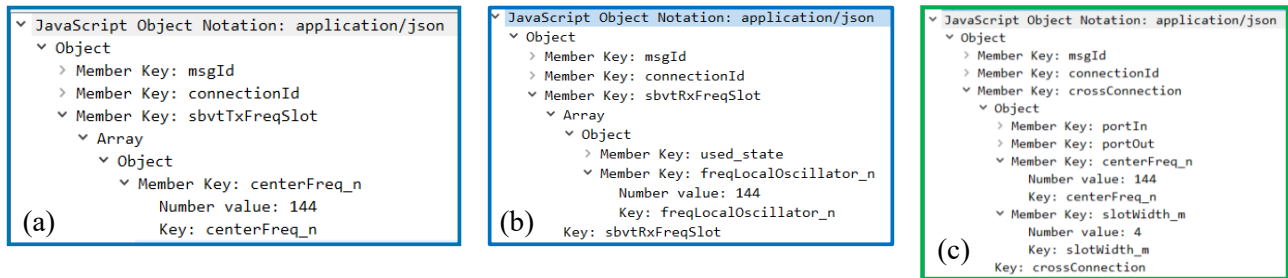

Figure 20 – Example of JSON for S-BVT Tx (a) Rx (b) and node (c) configuration.

6.3 EXPERIMENT 2 – INTEGRATION OF THE SDN CONTROLLER WITH THE TRANSMITTER AGENT

The aim of this experiment was to validate the integration of the CTTC SDN controller with the API described in [Mar20], referred to as SouthBound Interface (SBI), to support the automatic programmability of the underlying VCSEL-based SBVT transmitter. Such an optical device is controlled by a deployed SMO agent. In other words, the CTTC SDN controller interacts with the

PHOTONICS PUBLIC PRIVATE PARTNERSHIP

SMO SBVT Transmitter agent to: i) retrieve the status of the SBVT's VCSELs; ii) allocate or de-allocate SBVT's VCSEL as for the incoming optical connections.

This validation was conducted experimentally at the control plane level without entailing eventual real SBVT Transmitter configuration. However, it constitutes a necessary achievement to ensure the final end-to-end integration involving control and data plane elements.

The API for configuring the SBVT Transmitter agent was formerly defined in [Mar20] to be based on a REST API with JSON data encoding. However, the API has been extended to support both: REST and RESTCONF. For this specific experiment between the CTTC SDN controller and the SMO agent, the selected API is based on RESTCONF.

Remote Connectivity between CTTC and SMO

Figure 21 shows the schematic of the created VPN over Internet to allow the connectivity between both sites: CTTC in Castelldefels (Barcelona) and SMO at Milano. To this end, OpenVPN software package is used. At CTTC it is configured both the OpenVPN server and a client instance, whilst at SMO it is host a client instance. The used Public IP addresses are omitted for confidentiality reasons, and it is only shown the private IP addresses of the involved entities (i.e., SDN controller and agents) involved in the setup.
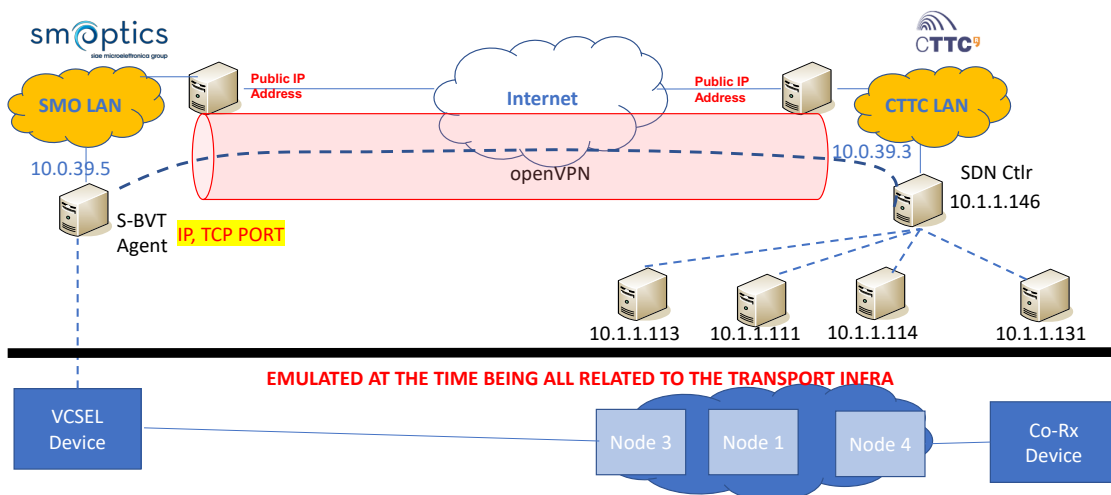

Figure 21. Schematic of the remote VPN-based connectivity between CTTC and SMO premises.

To validate the targeted integration the following entities are considered:

- SDN Controller (@CTTC) IP Address: 10.1.1.146
- SBVT Transmitter Agent (@SMO) IP Address: 10.0.39.5
- SBVT Receivers Agent (@CTTC) IP Address: 10.1.1.131
- Node1, Node3 and Node4 (@CTTC) IP Addresses:10.1.1.111, .113 and .114

Validation Execution

The objective is to, at the control plane level, request to the SDN controller an optical connection between the S-BVT Transmitter (@SMO) and the S-BVT Receiver (@CTTC) traversing the path formed by node3, node1 and node4. This optical connection is allocated in the centre frequency at 192.400 THz which corresponds to the ITU-T flexi-grid n=176. The slot width is set to m=4 entailing a 50GHz.

Figure 22 shows the control interactions (workflow) between the SDN controller and the agents locally managing the S-BVT devices and network nodes. Upon receiving the optical connection request at the SDN controller (step 1), this triggers the programmability (step 2) of the selected VCSEL source (n=176) at the S-BVT Tx (step 2). To do this, a RESTCONF-based POST method is sent by the SDN controller to the agent located at the SMO premises. Next, in step 3, it is configured the local oscillator (n=176) at the S-BVT Rx via a REST-based POST method. The configuration of each involved node (i.e., node 3, 1 and 4) is sequentially (as shown in step 4) realized determining for each node the input and output ports as well as the frequency slot in terms of n=176 and m=4. Once all the involved network elements and devices are configured, the optical connection is considered as successfully established (step 5).
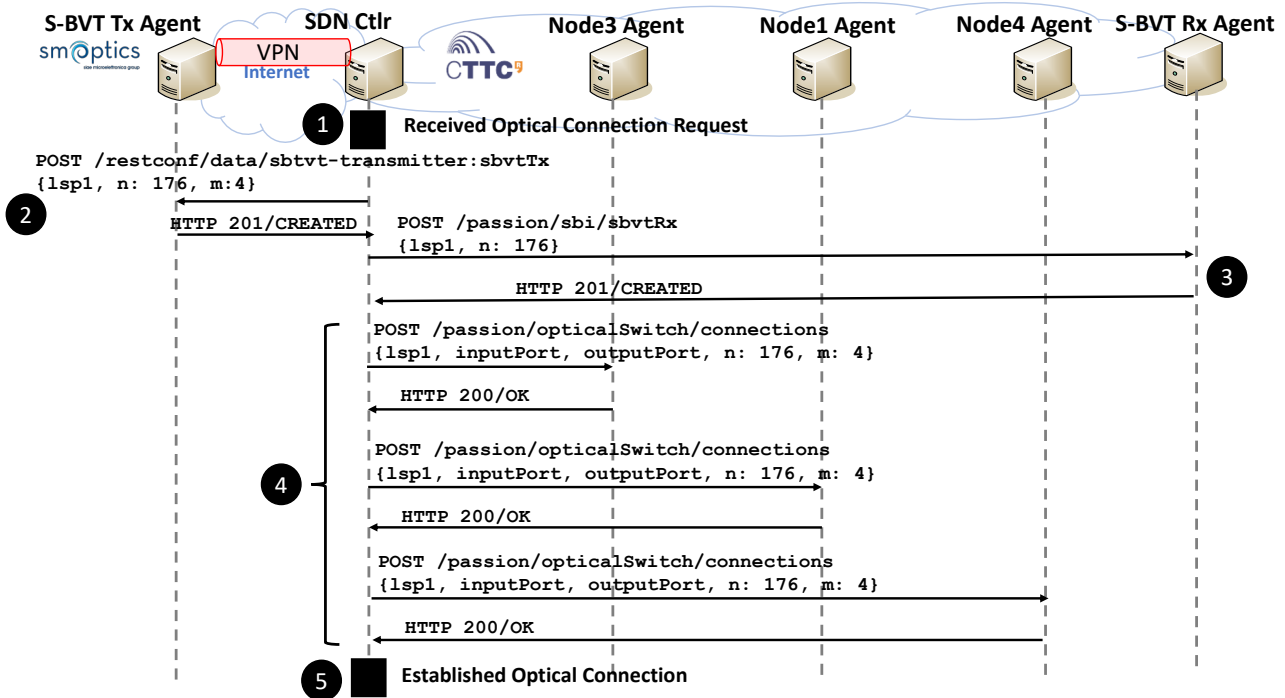

Figure 22. Workflow for setting up the targeted optical connection.

The above workflow has been validated experimentally as depicted in Figure 23(a). This illustrates using the Wireshark protocol analyser the exchanged control messages between the SDN controller and the agents managing the underlying network elements and devices involved in the optical connection. For the sake of completeness, those set of messages are labelled using the same steps numbering as used in Figure 22. Additionally, in Figure 23(b), (c) and (d) it is shown the JSON contents needed to allow programming the S-BVT Tx (with the VCSEL source set to n=176, m=4), S-BVT Rx (with local oscillator set to n=176) and optical node (with the frequency slot cross-connection determining the input and output ports along with the n=176 and m=4).

6.4 EXPERIMENT 3 – AUTONOMOUS SDN-BASED GLOBAL CONCURRENT RESTORATION

This experiment focuses on assessing a deployed autonomic networking capability assisting the implemented SDN controller [Mar21] to handle the dynamic restoration of optical connections. To

this end, it is implemented the Operational, Administration and Maintenance (OAM) entity. The OAM processes potential monitored information from the underlying optical metro network. Such a processing allows the OAM determining whether a network anomaly (e.g., link failure) occurs, and thus, resolve the optical connections being affected (e.g., disrupted). Hence, the AM of the OAM is to tackle the required actions to continuously preserve the transport services, i.e., restore the affected optical connections.
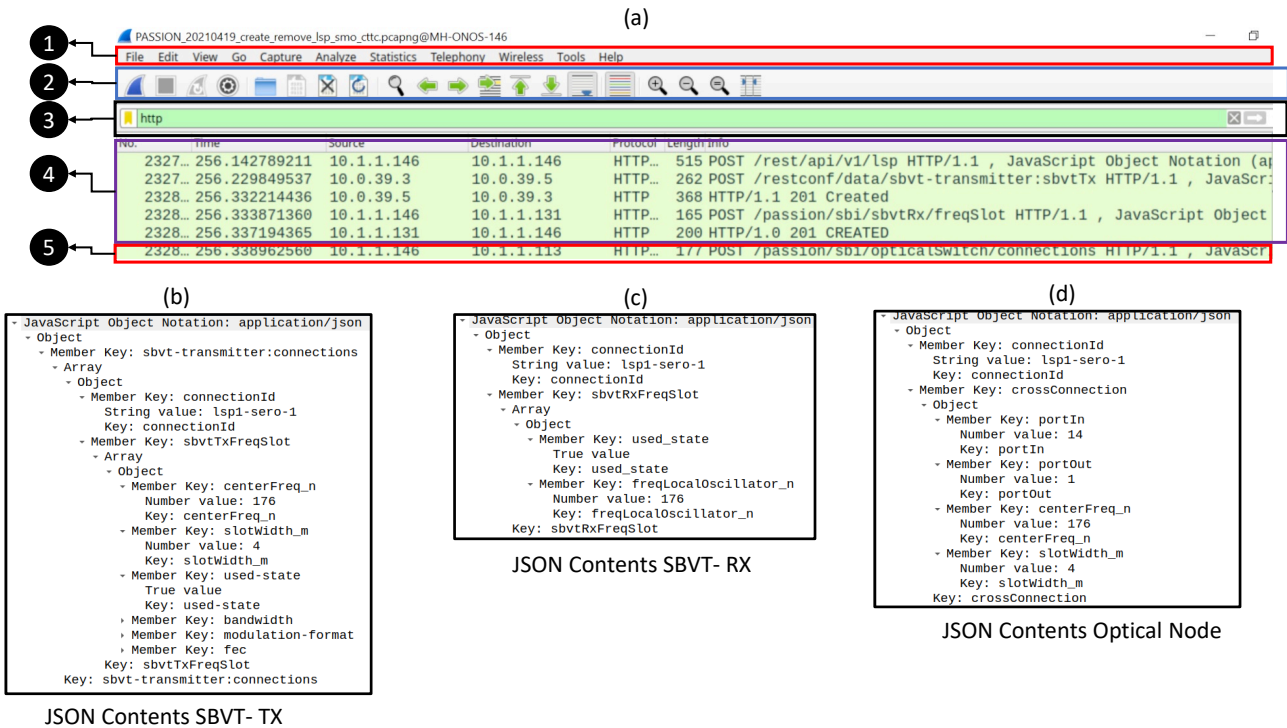

Figure 23. Wireshark captured control packets and JSON contents: (a) SDN Controller-Agents exchanged messages for setting up the optical connection; (b) Received JSON contents at the SBVT Tx Agent for configuring the VCSEL source;(b) Received JSON contents at the SBVT Rx Agent for configuring the local oscillator; (d) Received JSON contents for configuring the Node Agent cross-connection.

To deal with the above objective, Figure 24 depicts the SDN controller-OAM integration to support autonomic networking functions: S0) the regular allocation of new incoming optical connections specifying the source node (src), destination node (dst) and data rate (bw); S1) the collection of monitored information of established label switched paths (LSPs); S2) the training and testing mechanisms of machine learning (ML) models to e.g., predict network anomalies; S3) the processing of network anomalies (e.g., link failure); S4) the re-computation of affected optical connections (also referred to as LSPs) by a network anomaly. Herein, we focus on the S0, S3 and S4 operations: LSP provisioning and restoration.

In this experiment, the specific focus is on the S0, S3 and S4 operations. For the S0 (i.e., provisioning of new optical connections arriving to the SDN controller), it is adopted the Routing and Spectrum Assignment (RSA) Algorithm called as RSA Co-Routed (RSA-CR) described in [Mar21]. In a nutshell, upon a new connection request specifying the source node, destination node, and required bandwidth, the RSA-CR seeks for a feasible route fulfilling the bandwidth demands along with satisfying the spectrum continuity and contiguity constraints. The output of the computed path is made up by: i) the VCSEL sources at the S-BVT Tx attached to the source node; ii) the Co-Rxs at

the S-BVT Rx attached to the destination node; iii) the set of nodes and links to be traversed along with the frequencies slots (FSs) to be allocated.
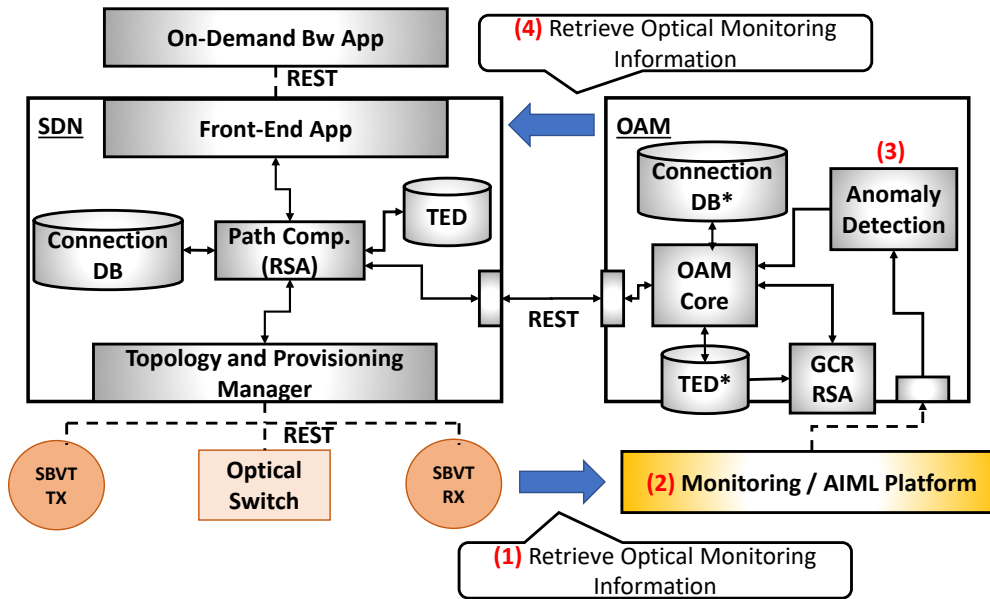

Figure 24. SDN Controller – OAM Interworking

It is worth recalling that the VCSEL source capacity reaches up to 50 Gb/s. Thus, connection demands with higher bandwidth requirements (e.g., 200 Gb/s) are accommodated over multiple flows bound to the same connection. These optical flows allocate different optical resources such as VCSEL sources, CO-Rxs, and FSs but are established over the same spatial path (i.e., nodes and links). This justifies the term of RSA co-routed since all the optical flows follow the same nodes and links. For the sake of completeness, as commented in [Mar21], the net data rate attained at the destination nodes for particular optical flows may be lower than 50 Gb/s. This is due to the accumulated impairments through traversing different nodes and links. To consider this, the RSA-CR algorithm applies different operational modes (OMs) for the data rate offered by the VCSEL sources which depend on both the path distance and number of hops. Accordingly, three OMs are defined: *high*, *medium*, and *low* whose data rates (Gb/s), maximum distance (in km) and maximum number of hops are determined in Table 7

Table 7 VCSEL Operational Modes (OM)

VCSEL Operation Mode (OM)	Data Rate (Gb/s)	Maximum Path Distance (km)	Maximum Number of Hops
High	50	30	5
Medium	40	75	9
Low	25	150	15

For the S3 operation, the implemented OAM tackles the actions upon a network anomaly arises. In this experiment, we only focus on link failures. After a link failure has been declared, the OAM performs three functions: i) determining the set of affected LSPs (i.e., *failedLSPs*); ii) the path and resource re-computation, iii) the allocation triggering of the computed LSPs via the SDN controller.

To do that, the OAM keeps a local duplication of both repositories: the connection database (DB) and the traffic engineering database (TED) When restoring *failedLSPs*, the OAM relies on a break-before-make (BBM) strategy where first all the f*ailedLSPs* are torn down, and then a devised RSA algorithm called Global Concurrent Restoration (GCR RSA) is executed to set up the successfully restored LSPs (out of the *failedLSPs*).

Description of the GCR RSA Algorithm

The main objective of the GCR RSA algorithm is to compute a feasible spatial and spectral path for each LSP in the *failedLSPs* maximizing the restorability. The restorability is defined as the ratio between the total successfully restored bandwidth and the total failed bandwidth. This the higher is such a ration, the better is the attained restorability. The GCR RSA is based on the above RSA-CR algorithm. The inputs of the GCR RSA algorithm are the *failedLSPs* formed by N LSPs (i.e., LSP1, LSP2, …, LSPn), and the gathered TED and SBVT information queried to the SDN controller. For each LSP_i, having its own src_i, dst_i, and bw_i, the GCR RSA algorithm executes the RSA-CR. The RSA-CR computations are done following the LSP ordering in the *failedLSPs*. Thus, prior to compute the next LSP_{i+1}, those selected resources (i.e., S-BVT VCSELs and CO-Rxs, and optical spectrum link) used to accommodate the LSP_i are set to occupied in the OAM's TED instance. This does avoid double-booking the same resources among LSPs, but the restorability success of the algorithm highly depends on the actual *failedLSPs* ordering. In other words, for a given *failedLSPs* there may be a specific ordering which does attain the highest restorability among those LSPs. Thus, the GCR RSA algorithm aims at exploring up to S (S≤ N!) solutions (i.e., S RSA-CR computations for each LSP) for a specific *failedLSPs*. Each s_i in S is computed shuffling/randomizing the LSP ordering. The final selected s_i is the one attaining the higher amount of restored bandwidth. If two or more solutions achieve the same amount of restored bandwidth, the chosen s_i is the one restoring the higher number of LSPs. If the tie holds, it is fostered the s_i leading to allocate the lowest amount of FSs among all the restored LSPs. Random selection is finally applied if the tie between two or more s_i still holds.

Experimental Validation and Evaluation

Figure 25 depicts the SDN controller-OAM workflow to restore a *failedLSPs* set. This entails 6 steps: R1) OAM connection DB retrieval of active LSPs via REST GET method sent to the SDN controller; R2) determining the failedLSPs; R3) releasing the LSPs in failedLSPs (via REST DELETE method); R4) querying via REST GET method an update of the TED and S-BVT resources; R5) executing the GCR RSA algorithm; and finally, R6) requesting the programmability of the successfully computed LSPs sending a POST message to the SDN controller. The contents of this specify: the LSP identifier, source node, destination node, and bandwidth along with describing the resources to be configured: nodes, links, and ITU-T flexi-grid FSs (64bits) in term of the central frequency (i.e., n) and slot width (i.e., m). This allows the SDN controller configuring the underlying optical network elements and devices (i.e., S-BVT VCSELs, CO-Rxs and optical switches).

The GCR RSA algorithm is experimentally evaluated upon both dynamic LSP arrival/departure, and network link failure events. The metro network topology (shown in Figure 26) is deployed over the CTTC ADRENALINE testbed with 28 Linux-based servers hosting S-BVTs and optical switch agents, and two servers for both the SDN controller and the OAM entity. Each access-metro network node (labelled by 1-24) has an S-BVT with 20 VCSELs (spaced 100GHz) and CO-Rxs. Transit nodes 25-27 form a 3 node-ring network for optical transport and aggregation between the access-metro and the metro-core node (labelled by 28). Node 28 has 3 S-BVTs supporting 160 VCSELs (spaced 25GHz) and CO-Rxs each. Optical links have different distances with 645 central frequencies spaced 6.25 GHz. New LSPs arrive according to a Poisson process with mean inter-arrival time (IATp) of

5s. The LSP duration is modelled exponentially with a mean holding time (HT) of 400, 500 and 600s. 5k unidirectional LSPs connecting either access-metro nodes to metro-core node (and vice versa) are requested whose bandwidth is uniformly distributed [50, 100, 150 and 200] Gb/s. Link failures occur exclusively within the 3-node ring using a Poisson process with an IATr set to 40s.
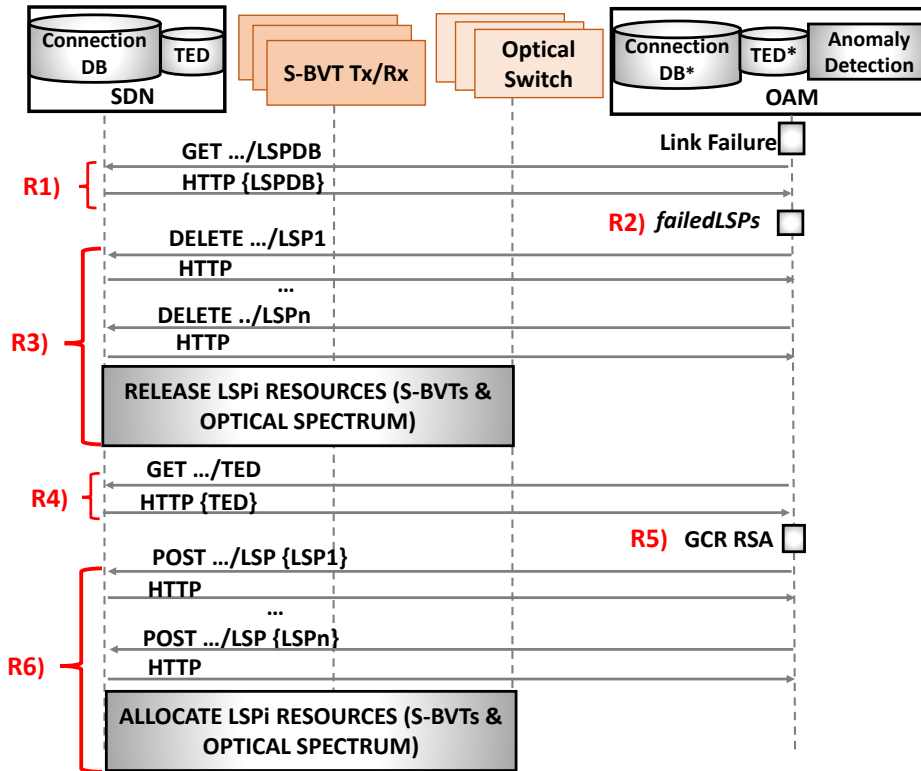

Figure 25. Workflow SDN Controller-OAM

Table 8 shows the performance evaluation comparing the GCR RSA algorithm when for each *failedLPs* it is computed a single solution (no shuffling), i.e., S=1, or adopting shuffling to derive up to 6 solutions (S=6). The performance metrics are the bandwidth blocked ratio (BBR), the average setup time (ST) in ms, the restorability, and the restoration time (RT) in ms. We observe that for low/medium traffic loads (i.e., low HT) increasing the number of explored solutions (i.e., S) by the GCR RSA algorithm, both the restorability and BBR are improved. For instance, for HT=400s, the BBR in S=1 is 0.08 whilst the same metric for S=6 results 0.065. For the restorability, S=1 achieves 0.86, whilst in S=6 this is 0.90. Indeed, as expected, S=6 fosters finding an existing solution that not only does enhance the restoration of larger amount of failed bandwidth, but also allows seeking for LSP paths which accomplish a more efficient use of the overall resources (i.e., lower amount of required S-BVT devices and FSs). This is done, however, at the expenses of increasing the restoration time due to higher computational time bound to a larger number of explored solutions. At high traffic load (HT=600s), both S=1 and S=6 performs similarly. Indeed, network resources tend to be notably occupied which severally constrains the number of feasible paths. Hence, exploring larger number of solutions by the GCR RSA algorithm does not bring an improvement in the targeted metrics.
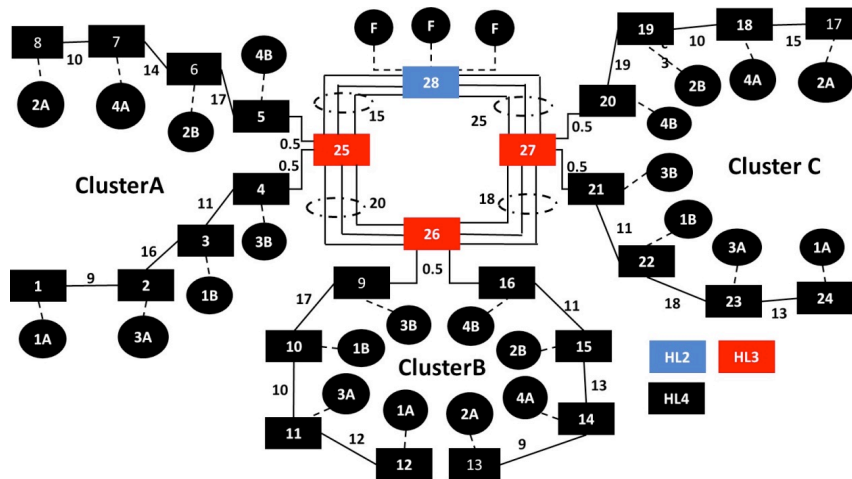
Figure 26. Optical Metro Network Scenario

This description of both the autonomous and integrated architecture of the SDN controller and OAM entity as well as the GCR RSA algorithm and the obtained performance evaluation were submitted to the OFC 2021 and accepted as oral presentation [Mar21].

Table 8 Performance evaluation GCR RSA S=1 and 6

HT (s)	GCR S= 1				GCR S= 6			
	BBR	ST (ms)	Restorability	RT (ms)	BBR	ST (ms)	Restorability	RT (ms)
400	0.08	106	0.86	1090	0.065	108	0.90	1150
500	0.11	108	0.88	1040	0.093	108	0.903	1055
600	0.13	109	0.89	1030	0.13	109	0.89	1036

7 CONCLUSIONS

This report summarises the state of the art of the envisaged integration steps and demo activities.

More precisely, the project developed four testbeds in different sites. POLIMI testbed was mainly devoted to the transmission aspects providing an extensive analysis of all the propagation impairments and limitations. NICT was mainly involved in the evaluation related to the capabilities of the exploitation of multicore fibres to increase the total transported capacity. TUE testbed was fully devoted to characterise and test the add/drop/switching subsystems. In CTTC ADRENALINE testbed the VCSEL-based S-BVT adopting integrated coherent detection was demonstrated over different connectivity scenarios. This deliverable describes the different testbed setups and report integration and testing activities and results at each site.

Despite the difficulties due to the COVID-19 situation, the lockdown and limited access to the labs, as well as related delay and issues with components availability and subsystems development, different demos have been conducted in order to provide the proof of PASSION concepts, the maturity of PASSION technologies and the envisioned metro network validation.

8 REFERENCES

[Gatto21] A. Gatto et al. "Performance Impairments due to Inter-Core Crosstalk Dynamics in a 7-Core MCF-Based DMT-Modulated Link" in Proceeding CLEO 2021 paper Stu1E.

[Mar20] R. Martínez, et al., "Experimental Evaluation of an On-line RSA Algorithm for SDN-Controlled Optical Metro Networks with VCSELbased S-BVTs," in Proc. Optical Network Design and Modelling (ONDM), 18-21 May 2020, virtual event.

[Mar21] R. Martinez et al. "Autonomous SDN-based Global Concurrent Restoration for High-Capacity Optical Metro Networks" in Proc. OFC 2021.

[Sval20] M. Svaluto Moreolo et al. "Experimental Assessment of a Programmable VCSEL-based Photonic System Architecture over a Multi-hop Path with 19-Core MCF for Future Agile Tb/s Metro Networks," OFC 2020, March 2020, S. Diego, USA

[Sval1-21] M. Svaluto Moreolo et al., "SDN-controlled Photonic System Architectures for Tb/s MAN Connectivity", 22 VDE ITG Fachtagung, Photonische Netze, 19-20 May 2021 (virtual event)].

[Sval2-21] M. Svaluto Moreolo et al., "Multi-Tb/s Photonic Transceivers for Metro Optical Network Connectivity Evolution," SPIE Photonics West 2021, March 2021 (virtual event].

[Sval3-21] M. Svaluto Moreolo et al., "Demonstration of an SDN-enabled VCSEL-based Photonic System for Spectral/Spatial Connectivity in Disaggregated Optical Metro Networks", https://www.ofcconference.org/en-us/home/program-speakers/demo/].

[Rapis21] M. Rapisarda et al, Add-Drop Lossless Switch Node in Multi-Hop Multi-Tb/s Metropolitan Area Networks, in Proc. OFC 2021

9 ACRONYMS

API	application programming interface
AWG	arrayed waveguide gratings
BBR	bandwidth blocked ratio
BER	bit error rate
BL/PL	bit and power loadings
BTB	back to back
BVT	bandwidth-variable transceiver
CO-Rx	coherent receiver
CP	cyclic prefix
CRM	coherent receiver module
CSPR	carrier to signal power ratio
CUT	channel under test
CW	continuous wave
DB	connection database
DD	direct detection
DFB	distributed feedback laser
DM	directly modulated
DMT	discrete multitone
DSB	dual sideband
DSP	digital signal processing
DWDM	dense wavelength division multiplexing
ECL	external cavity laser
EDFA	Erbium-doped fiber amplifier
FPGA	field-programmable gate array
FS	frequency slot
GCR RSA	global concurrent restoration

HT	holding time
ICXT	inter-core crosstalk
InP	Indium Phosphide
LCCS	laser current control system
LO	local oscillator
LSP	label switched paths
MCF	multicore fibre
MCM	multicarrier modulation
MCS	multicast switch
ML	machine learning
NFV	network function virtualization
NL VE	non-linear Volterra equalization
OAM	operational, administration and maintenance
OM	operational modes
OSNR	optical signal to noise ratio
PAM	pulse amplitude modulation
PCB	printed circuit board
PD	photodiode
PDM	polarization-division multiplexing
PIC	photonic integrated circuit
PM	power meter
PSM	photonic switch module
PXC	photonic cross-connect
QPSK	quadrature phase-shift keyed
ROADM	reconfigurable add-drop multiplexers
RSA	routing and spectrum assignment
RT	restoration time
RX	receiver
SBI	south bound interface
S-BVT	sliceable bandwidth-variable transceiver

SDM	space division multiplexing
SDN	software defined networking
SiPh	silicon photonics
SNR	signal to noise ratio
SOA	semiconductor optical amplifier
SOI	Silicon on insulator
SSB	single sideband
ST	setup time
STATX	short-term average crosstalk
SW	software
SWT	switch
TED	traffic engineering database
TX	transmitter
VCSEL	vertical cavity surface emitting laser
WBL	wavelength blocker
WDM	wavelength division multiplexing
WSS	wavelength selective switch